CHAPTER 2

EARTHQUAKE HAZARD

TABLE OF CONTENTS

LIST OF FIGURES

LIST OF TABLES

2. EARTHQUAKE HAZARD

2.1. INTRODUCTION

2.2. TECTONIC SETTING AND SEISMICITY OF MARMARA REGION

The city of Istanbul is located in the Marmara region, which has a complex tectonic region and is one of the most seismically active regions of the Eastern Mediterranean. To get a better understanding of the seismicity and the tectonics of the area, it will be necessary to analyze the overall seismicity and tectonics of the Marmara region.

2.2.1. Tectonics and Overall seismicity of the Marmara region

West of 31.5°E toward the Marmara Sea region (Mudurnu / Akyazı) the North Anatolian Fault Zone (NAFZ) begins to loose its single fault line character and splays into a complex fault system. Based on low-resolution bathymetric data (e.g. Figure 2.2.1) and earthquake occurrences, several researchers have developed different tectonic models for Marmara Sea. Among those scientists Pınar (1943), Pfannenstiel (1944), Crampin and Evens (1986), Sengor (1987), Barka and Kadisky-Cade (1988), Wong et al. (1995) and Ergun and Ozel (1995) can be cited (Figure 2.2.2). In 1999, Le Pichon et al. developed a fault model based on the data collected in 1997 by the ship "MTA Sismik-1" (Figure 2.2.3). The original MTA fault map is illustrated in Figure 2.2.4. In 17 November 1999, TPAO (Turkish Petroleum Corporation) have commented on their collected data with a map (Figure 2.2.5).

Data obtained during the recent high-resolution bathymetric survey of the Ifremer RV Le Suroit vessel indicates that a single, thoroughgoing strike-slip fault system (Main Marmara Fault) cuts the Marmara Sea from east to west joining the 17.8.1999 Kocaeli earthquake fault with the 9.8.1912 Sarkoy-Murefte earthquake fault (Figure 2.2.6) The Main Marmara Fault is argued to be a very young structure (about 200,000 years old), cutting across the older structures that formed the present NNE-SSW extensional pull-apart morphology of the Marmara Sea. Between 28.8E and 27.4E (Yesilkoy) the Main Marmara Fault exhibits typical characteristics of a major strike-slip fault. The fault follows the northern boundary of the Çınarcık Basin between Yeşilköy and the entrance of the Gulf of Izmit. (Figure 2.2.7)

The strike slip character of fault is further evidenced by the fault mechanism solutions of the recent earthquakes associated with the fault as can be seen in Figure 2.2.8 (Karabulut, private communication). The other active faults of mostly extensional type are located in the southern part of the Marmara Sea and to the east of Dardanelles. Such as those associated with the formation of Kapidag Peninsula, Marmara and Imrali Islands. Sengör argues that the Main Marmara fault accommodates the main E-W strike-slip component of the overall regional deformation, while the South Marmara tectonic structures accommodate the relatively much smaller N-S extension.

The long-term seismicity and GPS measurements and geological data suggest that the northern strand (i.e. Main Marmara Fault) of the fault zone is more active than the other two southern strands (Barka, 1997). As of the GPS studies; Straub et al. (1997) used a dense

network of 52 Global Positioning System (GPS) sites to determine the velocity field and strain rate pattern at the Marmara Sea region. Straub et al. (1997) have computed the tectonic strain rate in the Marmara Region in the Marmara Region on basis of a dense network of GPS sites in four GPS campaigns between 1990 and 1996 (Figure 2.2.9). They calculated the detailed kinematic fields of crustal motion. Both the GPS and the neotectonic data manifest that most of the deformation occurs along a relatively narrow E-W oriented zone extending from the single fault trace of the NAFZ through the Gulf of Izmit, the Marmara Sea, the Sarkoy region, and the Gulf of Saros into the North Aegean Trough. The Yalova peninsula endures considerable deformation as well. No significant deformation was found on the Biga peninsula. Thus, the western part of the middle strand that crosses the Biga peninsula is either inactive or locked. The southernmost station shows an average rate of 22±3 mm/yr oriented westward relative to Istanbul (Eurasia) which about 20 mm/yr of this amount is taken up by the Main Marmara Fault. This value is indicative of the dextral strike-slip motion of NW Anatolia relative to the Black Sea.

It can be shown that, if aseismic creep is neglected, over a long time period, the seismic moment released by earthquakes balances the moment accumulated by the elastic strain. The inter-event period between large (characteristic) earthquakes in these segments are also consistently estimated by dividing the seismic slip estimated from the earthquake catalod by the GPS-derived slip rate of 22±3 mm/yr.

In the Marmara region, there are some potential seismic gaps. For example, along the middle strand from the Mudurnu Valley region to the Aegean Sea there has not been any significant earthquake for the last 400 years, except the 1737 earthquake, in the Biga peninsula (Ambraseys & Finkel, 1991). The most western portion of the southern strand has not ruptured since 1855, except two small segments, the Pazarkoy-Edremit and Yenisehir segments. During historical time a number of earthquakes occurred along the northern strand, especially in the Marmara Sea area. Recent seismicity maps indicate a potential seismic gap in the central part of the Marmara Sea. Ambraseys and Jackson (2000), based on the absence of large, damaging earthquakes along the northern shore of the Marmara Sea, define this area as seismically quiet. In short, in the Marmara region by looking at recent seismicity pattern, one can suspect that there might be some seismic gaps in this area (Barka, 1992), (Figure 2.2.10). Figure 2.2.11 shows long-term seismic activity of the Marmara region whereas Figure 2.2.12 illustrates the last ten years seismic activity.

Based on recent findings it is possible to provide a fault segmentation model for the Marmara Sea region as shown in Figure 2.2.13. This model is based on the tectonic model of the Marmara Sea, defining the Main Marmara fault, a thoroughgoing dextral strike-slip fault system, as the most significant tectonic element in the region. (Le Pichon et al, 2001). The segmentation provided relies on Le Pichon et al.'s discussion of several portions of the Main Marmara Fault based on bathymetric, sparker and deep-towed seismic reflection data and interprets this discussion in terms of fault segments identifiable for different structural, tectonic and geometrical features. From east to west the Main Marmara fault cuts through Cınarcık, Central and Tekirdag basins, which are connected by higher lying elements. For instance the fault follows the northern margin of the basin when going through the Cınarcık trough in the northwesterly sense, makes a sharp bend towards west to the south of Yesilkoy, entering central highs, cuts through the Central basin and alternates in this manner until it reaches the 1912 Murefte-Sarkoy rupture. All these features are interpreted as different fault segments in our model.

2.2.1.1. Historical earthquakes that affected the Marmara Region, (Ambraseys & Finkel, 1991)

In Istanbul, earthquake records spanning two millennia indicate that, on average, at least one medium intensity (Io=VII-VIII) earthquake has affected the city every 50 years (Ambraseys and Finkel, 1991). The average return period for high intensity (Io=VIII-IX) events has been 300 years. Damage distribution in Istanbul as a result of 1509, 1766 and 1894 earthquakes is illustrated in Figure 2.2.14, Figure 2.2.15 and Figure 2.2.16. Description of damages in earthquakes between 32 and 1894 can be found in Appendix 1.

The earthquake damage experienced by the historical structures in Istanbul has been well documented. Figure 2.2.17 provides three-dimensional matrix of damage levels for important historical structures against earthquakes affecting Istanbul since 1500. In this illustration D1, D2, D3, D4 and D5 respectively stand for: Negligible to slight damage, Moderate damage, Substantial to heavy damage, Very heavy damage and Destruction. It can be seen that Fatih and Edirnekapi Mihrimah Sultan Mosques are highly vulnerable to earthquake damage and, unless precautions are taken can be heavily damaged in the next Istanbul earthquake. It is known that the Hagia Sophia Museum was affected by the earthquakes that took place in the region within the last five hundred years. Existing historical data do not allow for a detailed and correct quantification of damage to the building. However all these earthquakes caused damage in the building, which required subsequent repair and retrofit (Ambraseys, 1991).

Figure 2.2.18 (after Hubert-Ferrari, 2000) illustrates the sequence of earthquakes in the 18th century. It has been alleged that the 17.08.1999 earthquake may be associated with the 1719 earthquake of this sequence. Recent studies conducted after the 1999 Kocaeli (Mw=7.4) and Düzce (Mw=7.2) earthquakes indicate (assuming that the stress regime in the Marmara Sea remains unchanged) about 65% probability for the occurrence of a Mw>=7.0 magnitude earthquake effecting Istanbul as indicated in Figure 2.2.19 (Parsons et. al., 2000).

After detailed assessment of the distribution of reported earthquake damages, historical earthquakes that affected the Marmara Sea region between 1500-present have been connected with the fault segmentation model presented in Figure 2.2.13. Fault ruptures associated with the fault segmentation have been shown in Figure 2.2.20 through Figure 2.2.24 for time periods of 1500-1599, 1600-1699, 1700-1799, 1800-1899 and 1900-1999 respectively and have been summarized in Table 2.2.1.

Table 2.2.1. Association of earthquakes between 1500-present with the segmentation proposed for the Northern Portion of the North Anatolian Fault in the Marmara Region.

Earthquake	Fault Segment
10.9.1509 (Ms= 7.2)	7, 8
10.5.1556 (Ms=7.2)	9
25.5.1719 (Ms=7.4)	2, 3, 4, 5
2.9.1754 (Ms=6.8)	6
22.5.1766 (Ms=7.1)	7, 8
5.8.1766 (Ms=7.4)	11
10.7.1894 (Ms=7.3)	3, 4, 5
9.8.1912 (Ms= 7.3)	11
17.8.1999 (Ms=7.8)	1, 2, 3, 4

*See **Figure 2.2.20** through **Figure 2.2.24** for an illustration of historical earthquakes and associated segmentation.*

2.2.1.2. Recent Seismic Activity in the Marmara Region

Earthquakes in the Marmara region have been relatively few in the 20th century. Detailed descriptions of the major events are given below. Fault segment numbers that are based on the new segmentation presented in Figure 2.2.13, and are associated with earthquakes that took place in the region in the 20th century are provided in parenthesis following the description of each earthquake.

1909 October 9 Karamürsel Earthquake, Ms = 5.8, Io = VII

The earthquake caused considerable damage in Koglacik region located between Izmit Bay and Iznik Lake. Two more shocks with approximately the same magnitude followed the first event. Several houses and churches have been damaged by the events. The shocks were also felt in Çatalca, Terkos, Istanbul, Göynük, Bolu and Bursa (Ambraseys and Finkel, 1987b).

1912 August 9 Murefte-Sarkoy Earthquake, 40.50N - 27.00E, Ms = 7.4, Io = X

This earthquake destroyed more than 300 villages and towns mainly to the north of the Dardanelles, killing over 2000 people. The shock was associated with a 50 km long fault-break and with the liquefaction of the ground up to epicentral distances of 180 km. Damage extended over a relatively large area and long-period ground motions were responsible for serious damage to public buildings as far as Edirne and Istanbul. The shock was accompanied by a small seismic sea-wave and it was felt within a radius of about 450 km. The intensity distribution of the earthquake as given by Ambraseys and Finkel (1987a) is given in Figure 2.2.25 (Eyidogan et al., 1991). This earthquake can be associated with fault segment 11 (Figure 2.2.13 and Figure 2.2.24) (Ambraseys (2000), Hubert-Ferrari et al. (2000)).

1935 January 4 Erdek-Marmara Islands earthquake, 40.0 N – 27.5 E, Ms = 6.4, Io = IX

A destructive earthquake followed by three strong aftershocks occurred in Marmara Islands and Erdek and caused serious damage in several villages. The shock was also felt in Istanbul, Edirne and Izmir.

1953 March 18 Yenice-Gönen earthquake, 40.0 N, 27.3 E, Ms = 7.2, Io = IX

The earthquake is associated with the Yenice-Gonen segment of the southwestern strand of North Anatolian Fault. The earthquake mechanism is right-lateral strike-slip. The mapped surface break for this event was 50 km (Ketin and Roesli, 1953). The earthquake caused damage over a 30,000-km^2 wide area in northwest Anatolia between Marmara and North Aegean regions (Pınar 1943). The iso-seismic map of the event is given in Figure 2.2.26 (Eyidogan et al., 1991). This earthquake can be associated with fault segment 19 (Figure 2.2.13 and Figure 2.2.24) (Ambraseys (2000), Barka and Kadinsky-Cade (1988), Hubert-Ferrari et al. (2000)).

1957 May 26 Abant earthquake, 40.67 N, 30.86 E, Ms = 7.0, Io = IX

The earthquake occurred on the North Anatolian fault, rupturing the segment of the fault between Bolu and Akyazı. It was followed by the 1967 Mudurnu Valley earthquake in the sequence earthquakes rupturing the North Anatolian Fault in the 20th century. It caused

significant damage in the villages situated along the fault zone, whereas the damage was slight in Adapazarı and Abant.

1963 September 18 Çınarcık earthquake, 40.8 N, 29.1 E, Ms = 6.3, Io = VIII

The earthquake was strongly felt over a $70,000^2$ km area around the Marmara Sea. The shock was destructive in Cınarcık, Yalova and in neighboring villages and strongly felt in Kılıc, Armutlu, Mudanya and Gemlik. Slight damage has been observed in Istanbul and Bursa (Figure 2.2.27) (Eyidogan et al., 1991). The dominant component of the earthquake mechanism was normal.

1964 October 6 Manyas earthquake, 40.30 N, 28.23 E, Ms = 6.9, Io = IX

The earthquake occurred in the southern shores of Manyas Lake, south of Marmara Sea, having landslide and liquefaction effects and causing damage in Manyas, M. Kemalpasa, Gonen, Susurluk, Karacabey and Bandirma and it was strongly felt Istanbul. The earthquake mechanism was determined as normal. This earthquake can be associated with fault segment 18 (Figure 2.2.13 and Figure 2.2.24) (Ambraseys (2000), Barka and Kadinsky-Cade (1988), Hubert-Ferrari et al. (2000)).

1967 July 22 Mudurnu Valley earthquake, 40.67 N, 30.69 E, Ms = 6.8, Io = X

This earthquake was the preceding one of the 1999 Kocaeli event in the westward moving series of earthquakes that ruptured the whole length of the North Anatolian Fault between Erzincan and Izmit in the 20th century. The fault rupture was 80 km long between Sapanca and Abant Lakes. The right lateral displacements on the eastern 20 km, that had already ruptured in the 1957 Abant earthquake were in the range of a few cm, whereas the displacements reached 190 cm along the western segments of the rupture zone. Vertical displacements up to 120 cm were also observed. The isoseismal map of the earthquake as given by Ergin et al. (1971) is presented in Figure 2.2.28 (Eyidogan et al., 1991). This earthquake can be associated with fault segment 12 (Figure 2.2.13 and Figure 2.2.24) (Ambraseys (2000), Barka and Kadinsky-Cade (1988), Hubert-Ferrari et al. (2000)).
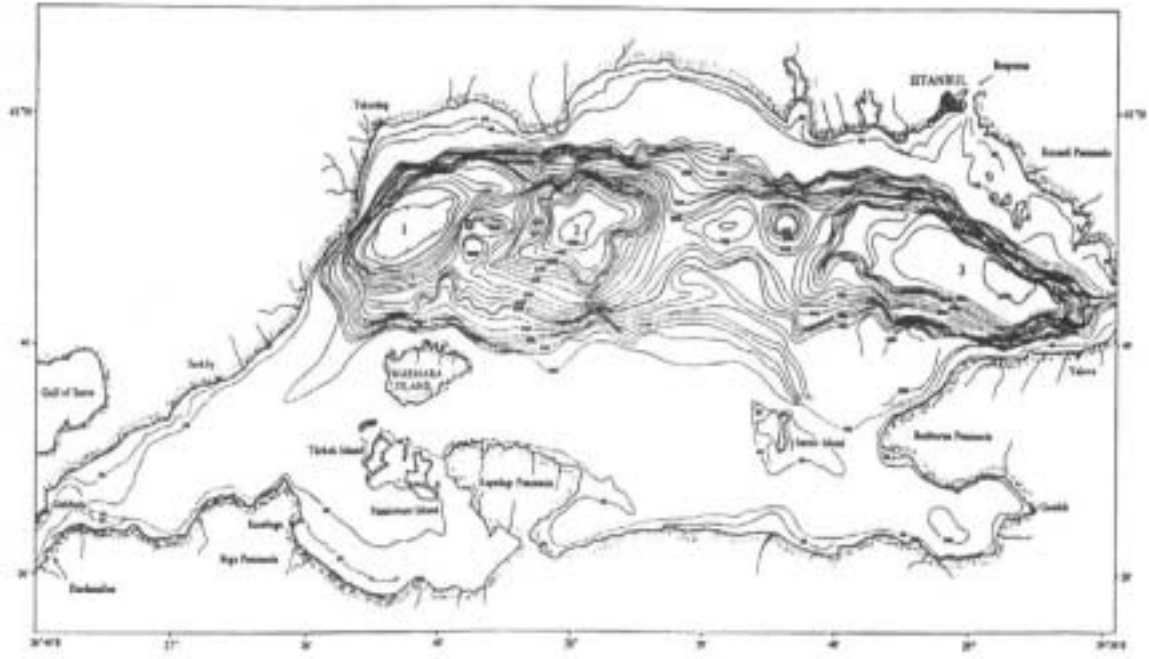
Figure 2.2.1. Bathymetry map of the Marmara Sea (Wong et al., 1995). The three deep basins are named as:1) Tekirdağ Basin, 2) Central Marmara basin, 3) Çınarcık Basin.
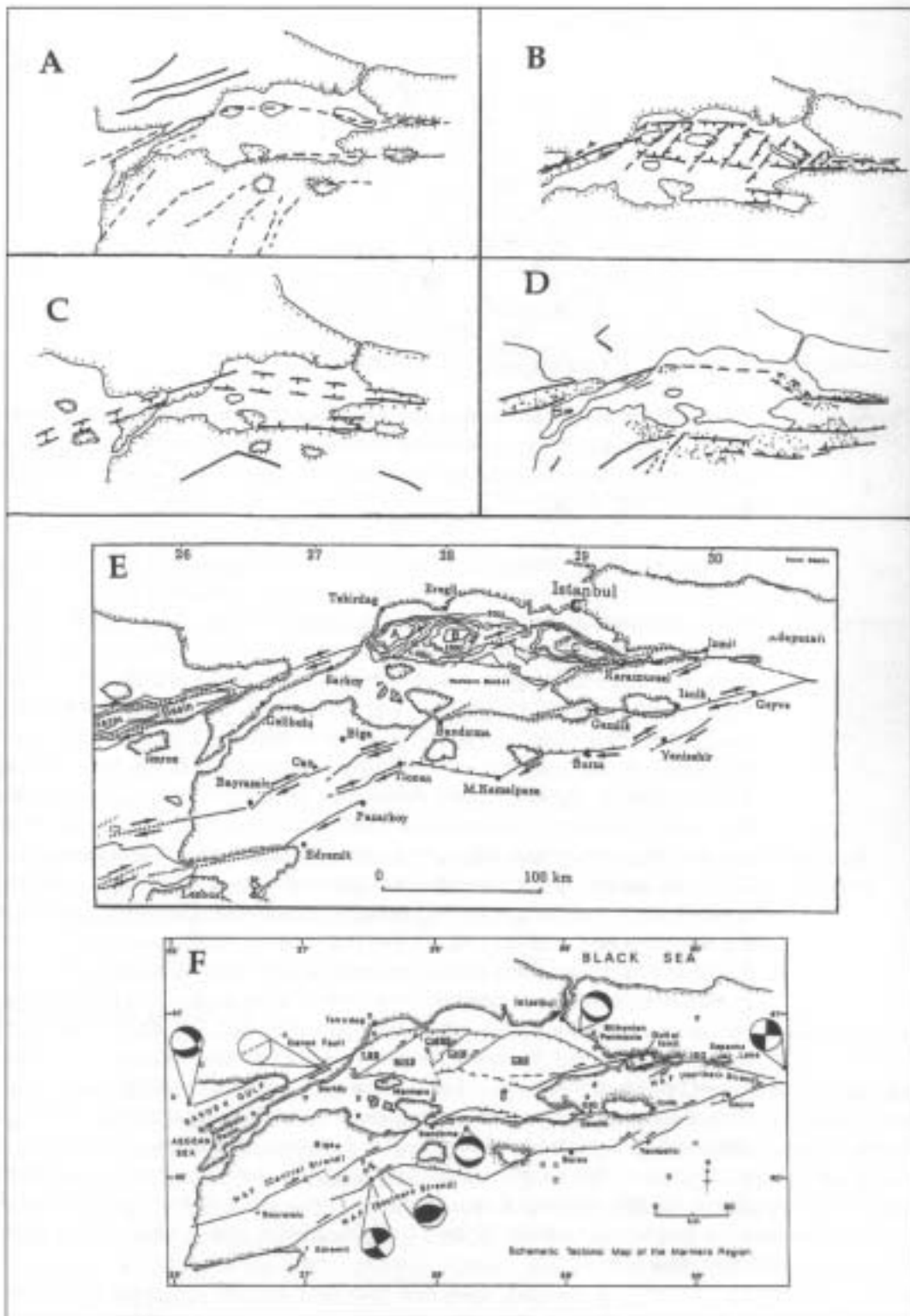
Figure 2.2.2. Comparison of the structural models suggested for the Marmara Region. (a) Pınar (1943), (b) Pfannenstiel (1944), (c) Crampin and Evans (1986), (d) Şengör (1987), (e) Barka and Kadinsky-Cade (1988), (f) Wong et al. (1995), Ergün and Özel (1995).

Figure 2.2.3. Le Pichon et al. (1999) developed a fault model based on the data collected in 1997 by the ship MTA Sismik-1.

Figure 2.2.4. The original MTA Sismik-1 fault map.
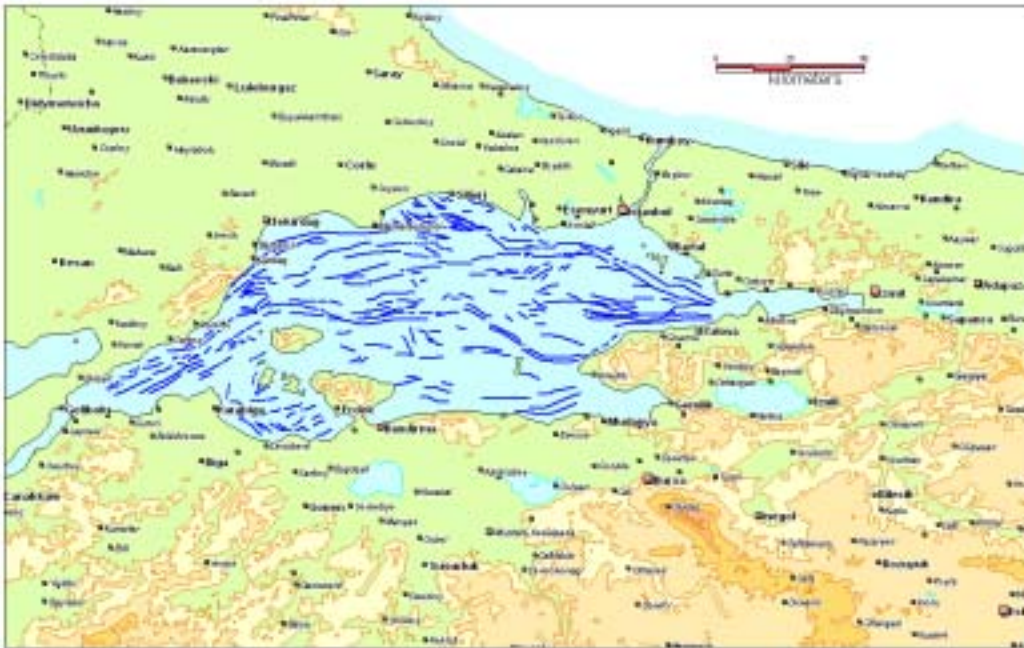
Figure 2.2.5. The Turkish Petroleum Corporation (TPAO) map(1999).
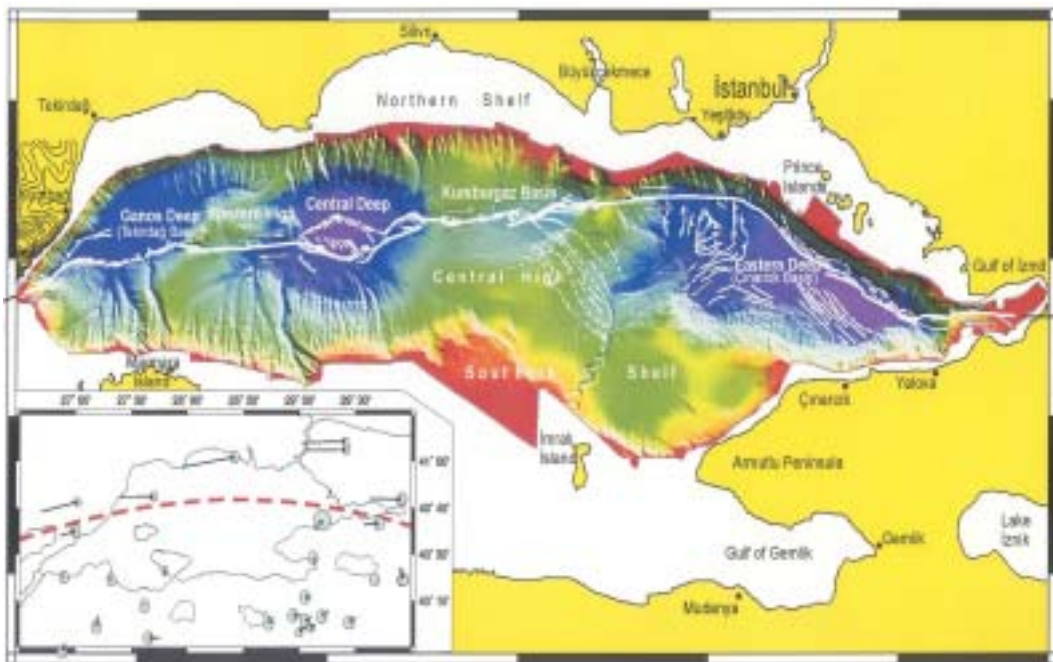
 Figure 2.2.6. The recent high-resolution bathymetric map obtained from the survey of the Ifremer RV Le Suroit vessel that indicates a single, thoroughgoing strike-slip fault system.

Figure 2.2.7. The"Main Marmara Fault" that follows the northern boundary of the Çınarcık Basin between Yeşilköy and the entrance of the Gulf of Izmit.
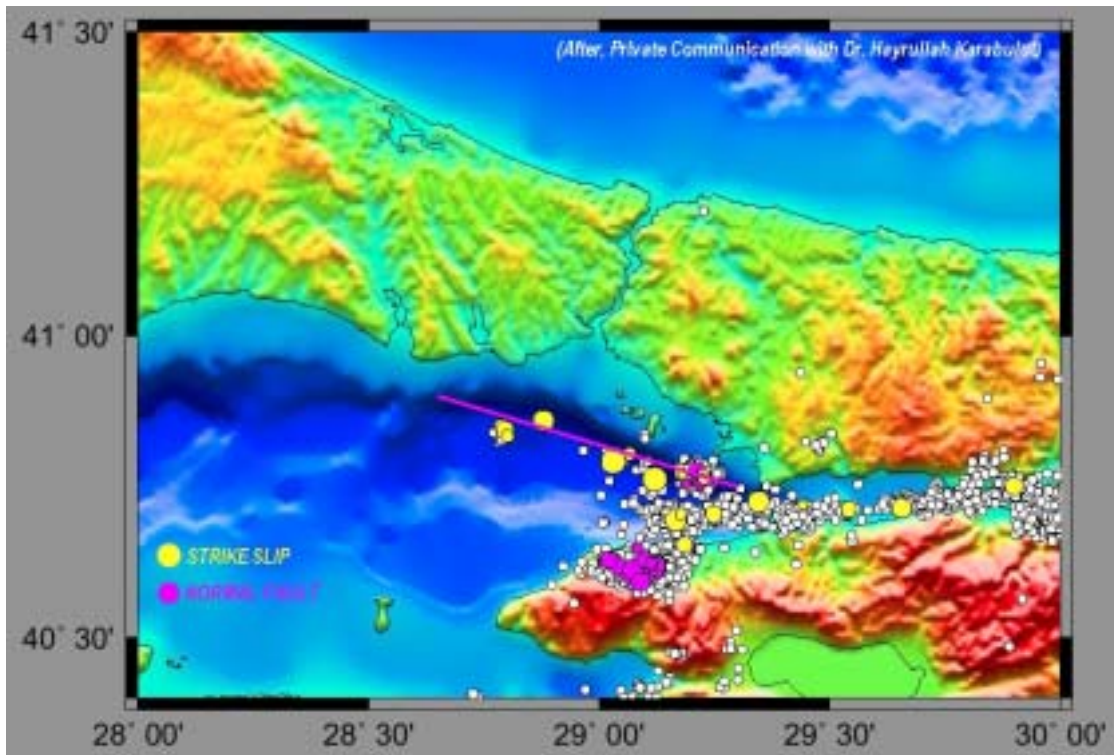
Figure 2.2.8. The fault mechanism solutions of the recent earthquakes associated with the fault (Ozalaybey et al., 2001).

21
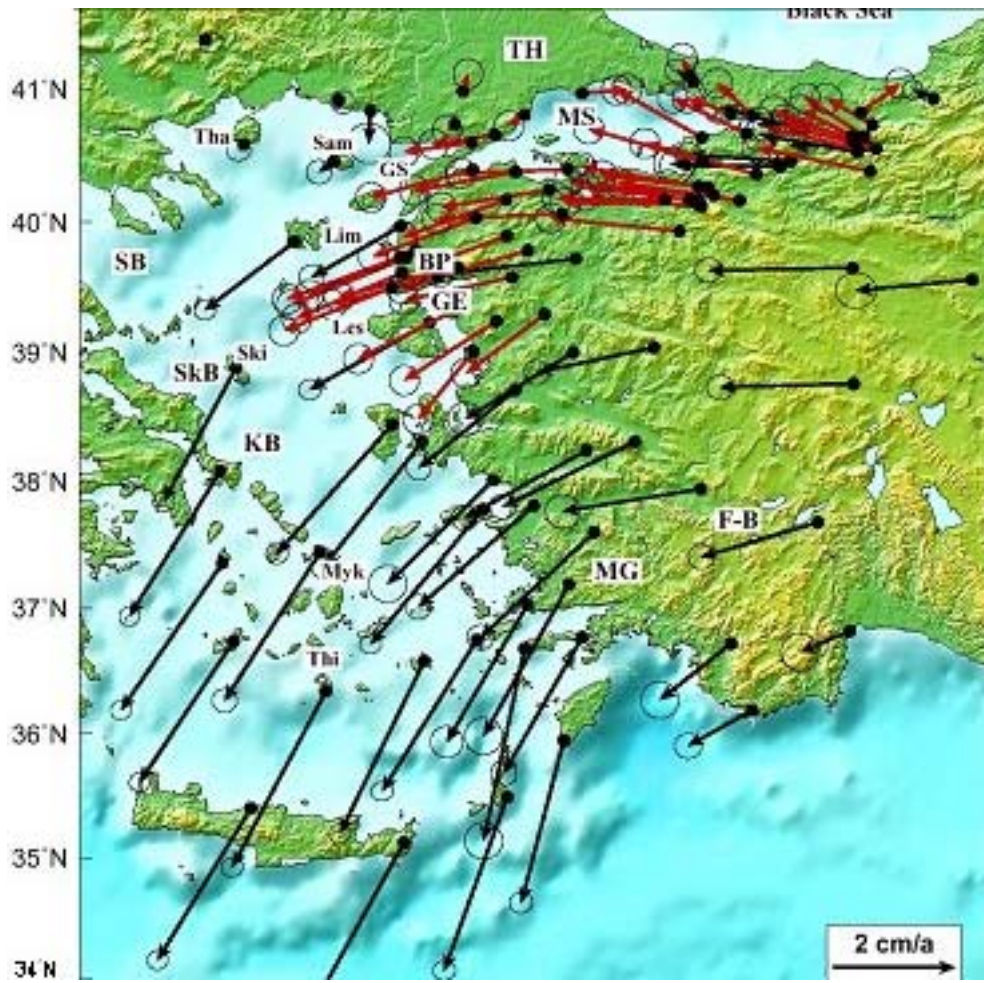
Figure 2.2.9. GPS based tectonic slip rates(After Straub et al, 1997).
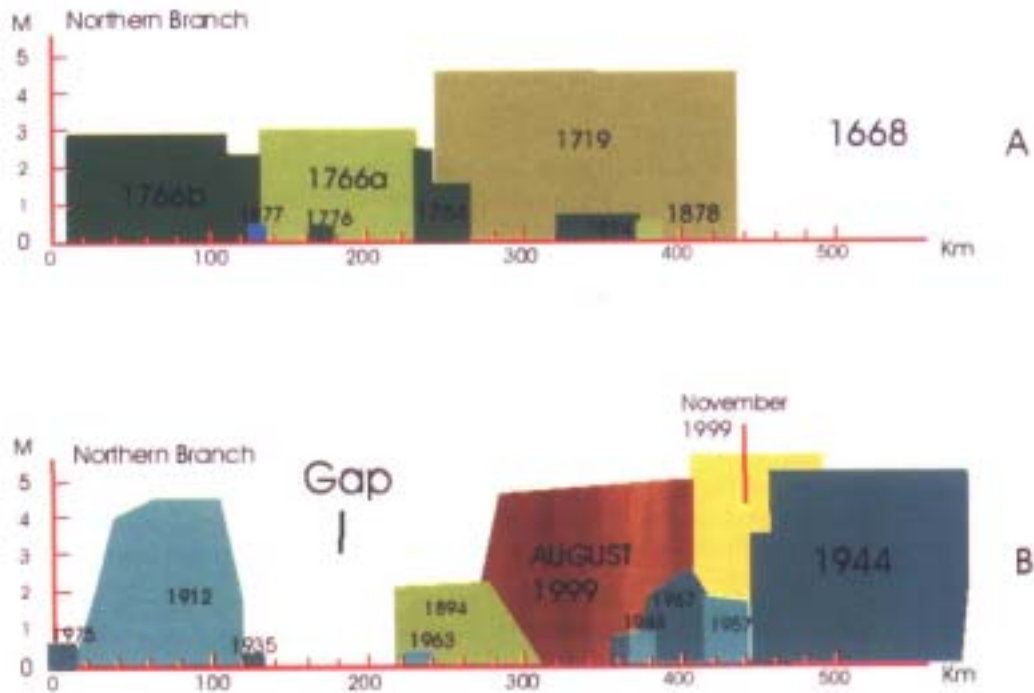
Figure 2.2.10. Earthquake activity along the northern strand of the North Anatolian fault since 1700 AD. (Modified from Hubert et al., 2000).
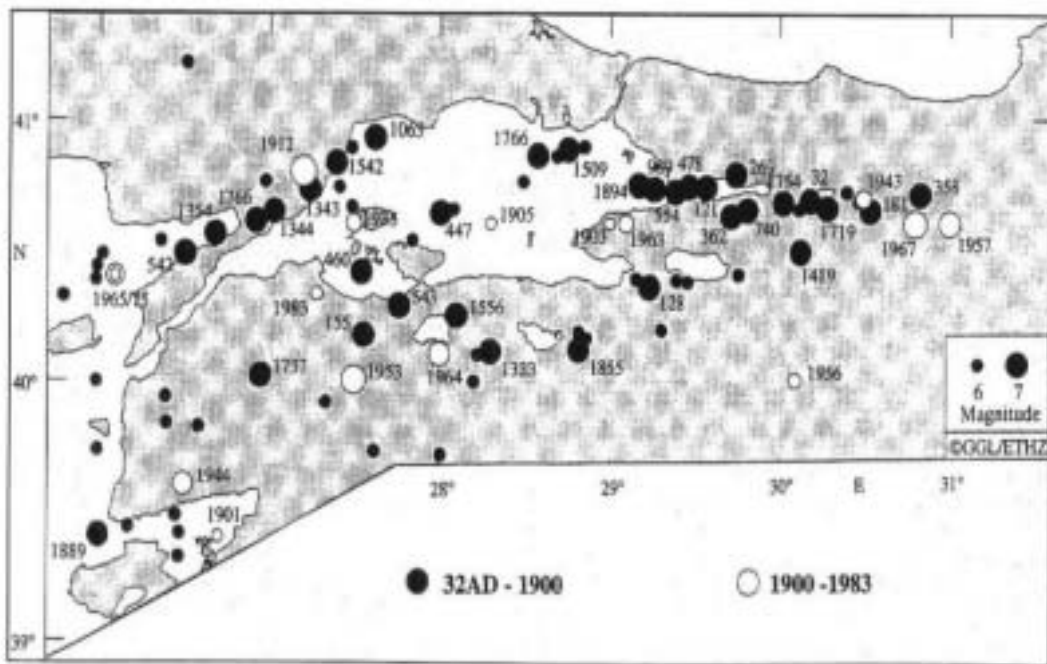
Figure 2.2.11. Historical Earthquakes in the Marmara Sea region, originally from Ambraseys and Finkel (1991), taken from Straub (1997).
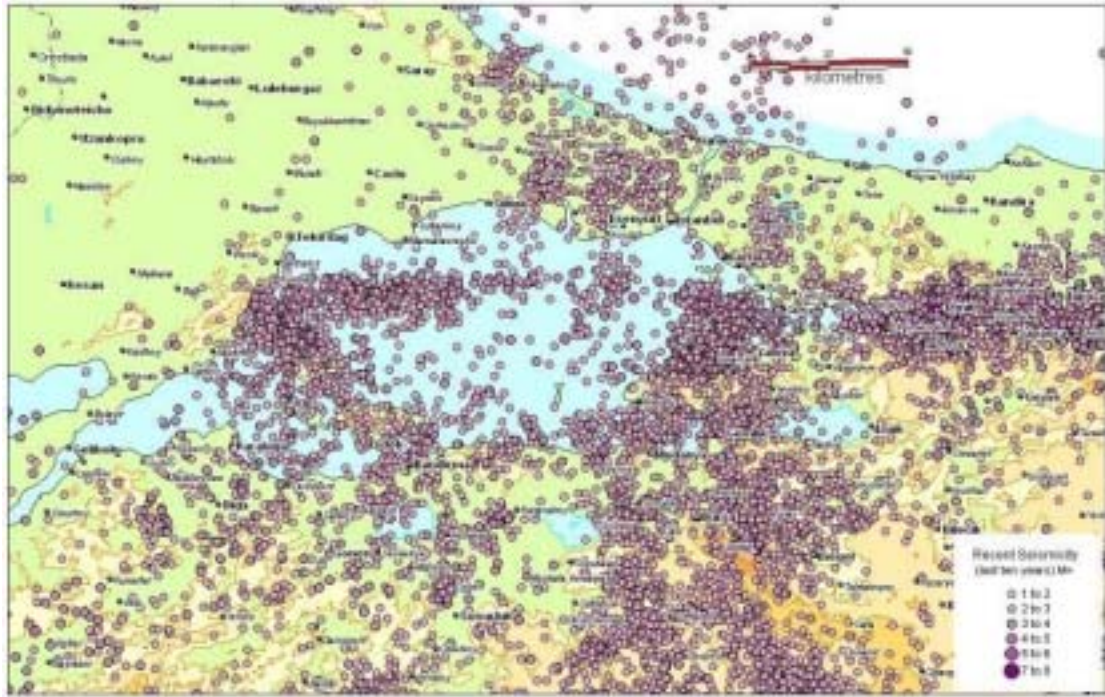
Figure 2.2.12. The seismic activity of the Marmara region with M>1 events for the last ten years.

Figure 2.2.13. The fault segmentation model for the Marmara region.

Figure 2.2.14. Historical structures of the ancient city of Istanbul damaged by the 1509 September 10 earthquake (compiled by Swift-Avcı, 1996).

Figure 2.2.15. Historical structures of the ancient city of Istanbul damaged by the 1766 May 22 earthquake (compiled by Swift-Avcı, 1996).
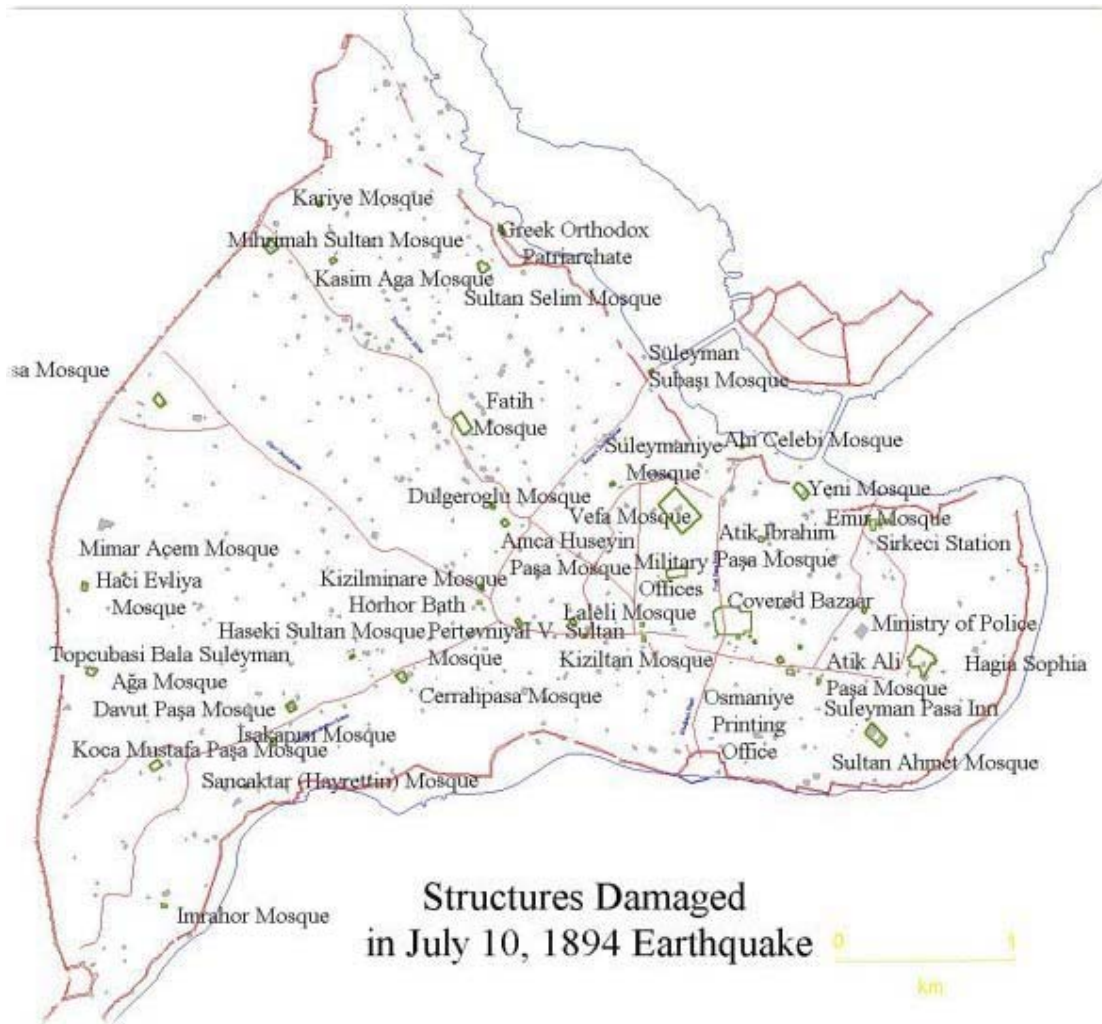
Figure 2.2.16. Historical structures of the ancient city of Istanbul damaged by the 1894 July 10 earthquake (compiled by Swift-Avcı, 1996).
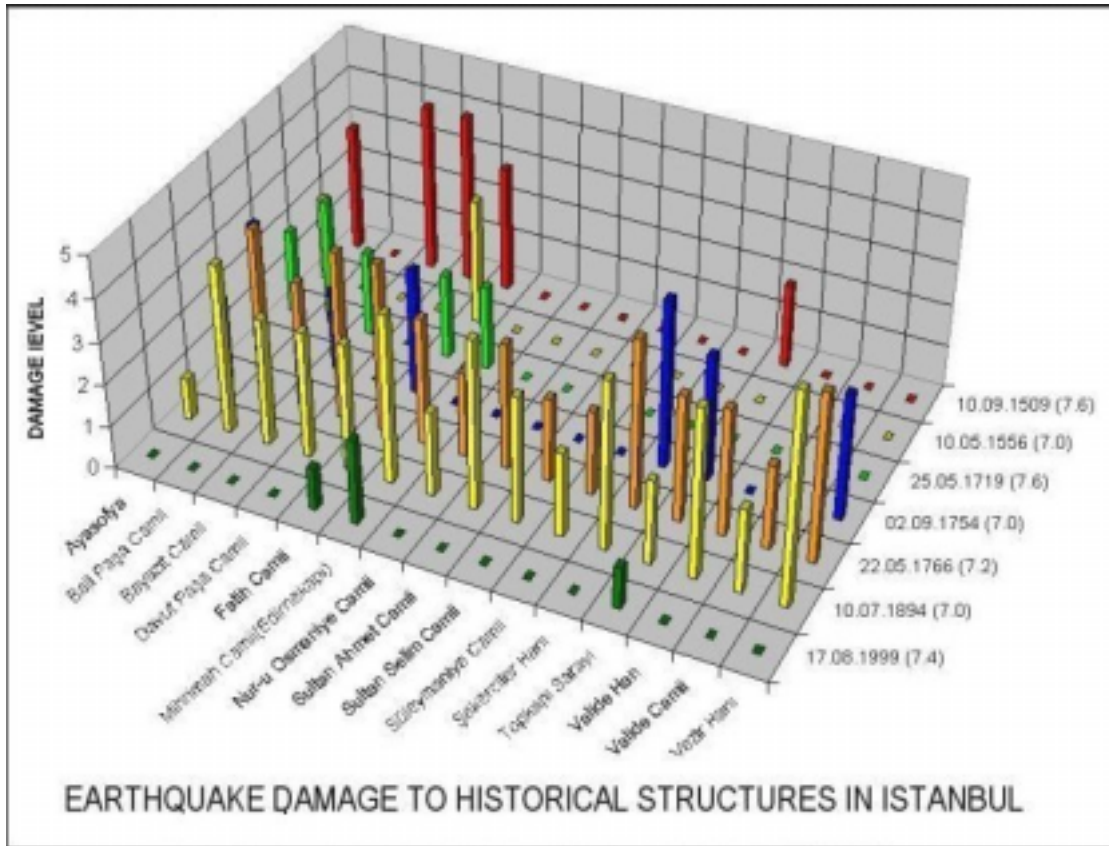
Figure 2.2.17. Damages sustained by important historical structures in earthquakes affecting Istanbul since 1500.
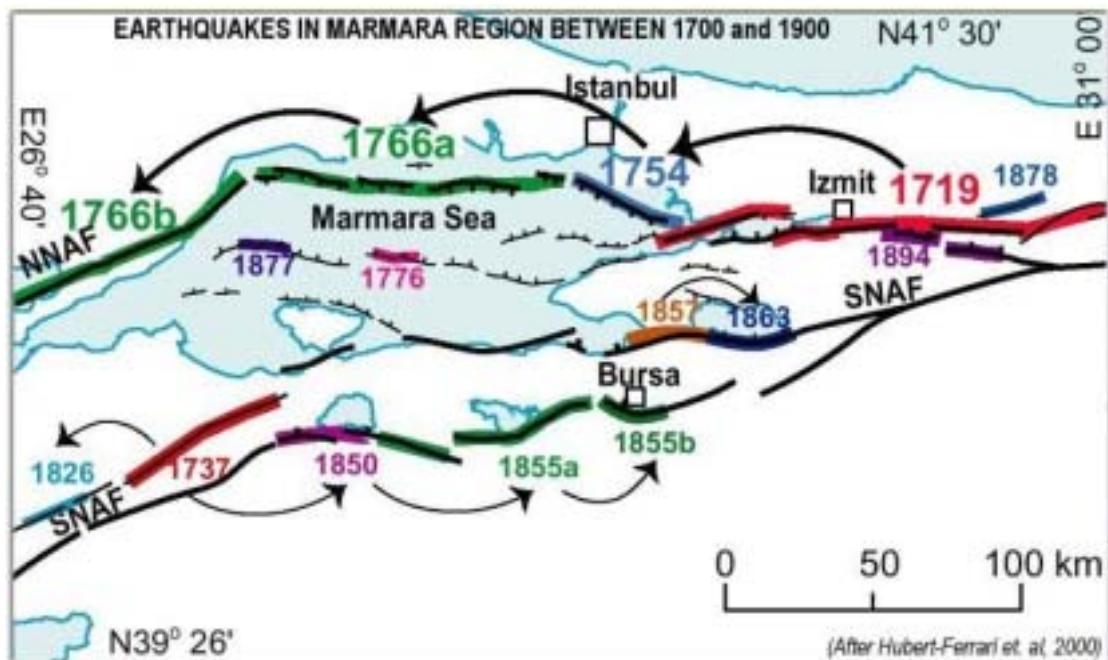
Figure 2.2.18. The sequence of earthquakes in the 18th century around Marmara region.
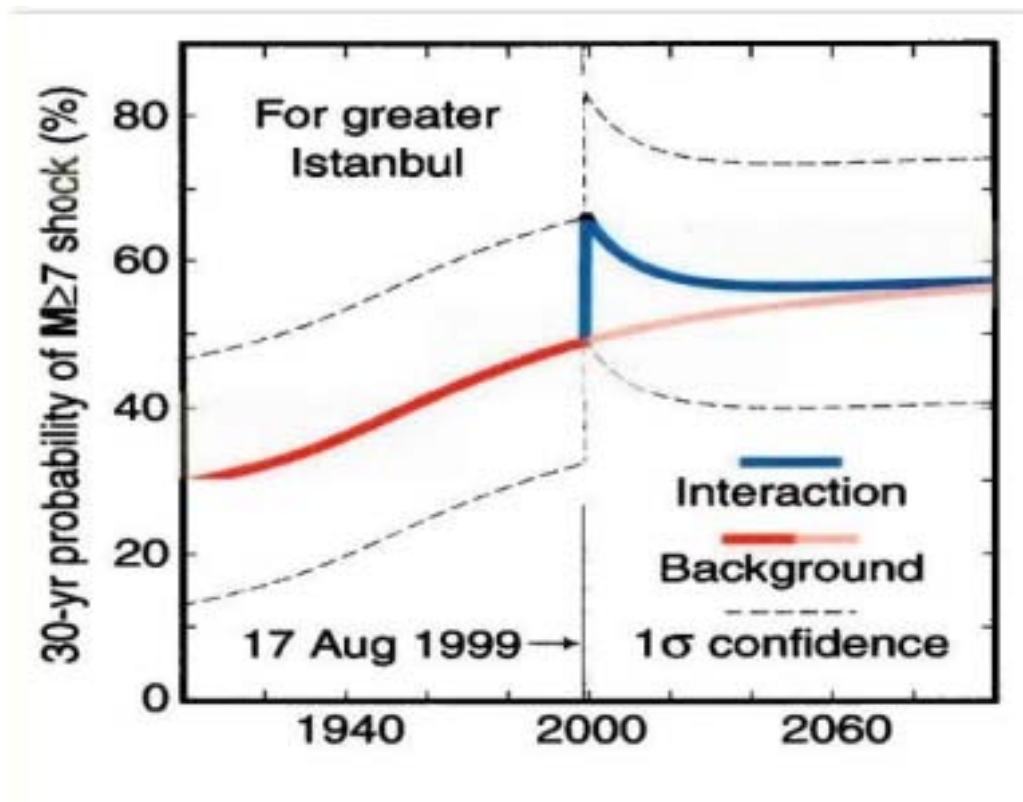
Figure 2.2.19. Probability for the occurrence of an Mw>=7.0 earthquake affecting Istanbul for the next 30 years (Parsons et. al., 2000).

Figure 2.2.20. Historical earthquakes between 1500-1599 associated with the fault segmentation model of the Marmara region.

Figure 2.2.21. Historical earthquakes between 1600-1699 associated with the fault segmentation model of the Marmara region.

Figure 2.2.22. Historical earthquakes between 1700-1799 associated with the fault segmentation model of the Marmara region.

Figure 2.2.23. Historical earthquakes between 1800-1899 associated with the fault segmentation model of the Marmara region.

Figure 2.2.24. The earthquakes between 1900-1999 associated with the fault segmentation model of the Marmara region.

Figure 2.2.25. Iso-seismal map of August 9, 1912 Şarköy-Mürefte earthquake.

Figure 2.2.26. Iso-seismal map of March 18, 1953 Yenice-Gönen earthquake.
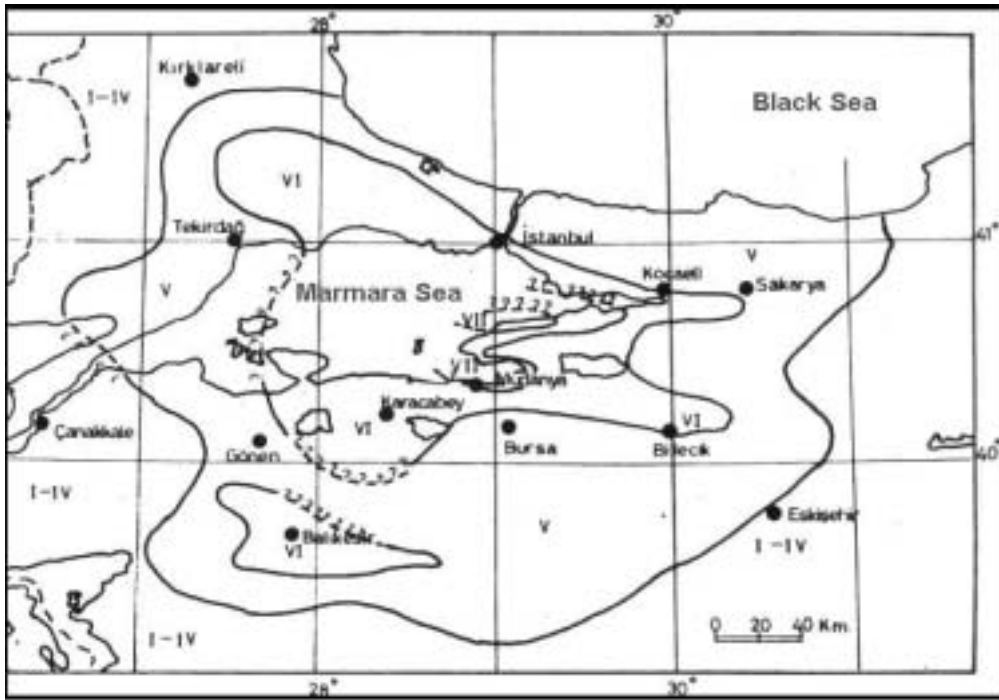
Figure 2.2.27. Iso-seismal map of September 18, 1963 Çınarcık earthquake.
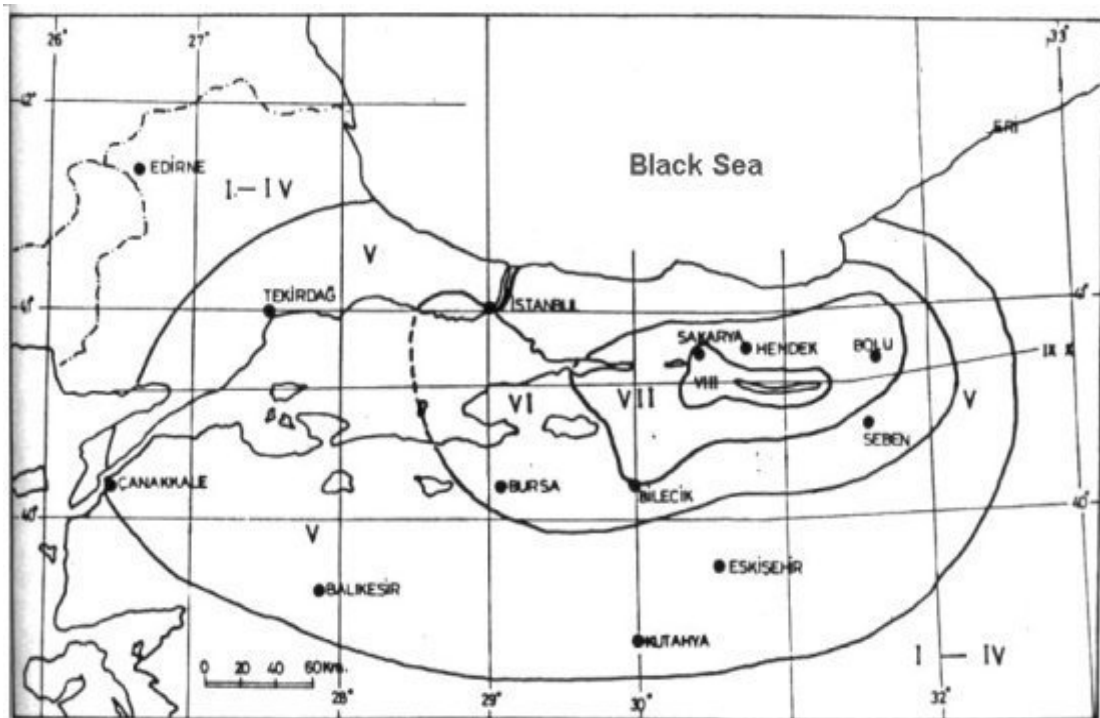
Figure 2.2.28. Iso-seismal map of July 22, 1967 Mudurnu Valley earthquake.

2.3. 17.8.1999 KOCAELI EARTHQUAKE

1999 August 17 Kocaeli earthquake, 40.702 N, 29.987 E, Mw=7.4

An earthquake of magnitude Mw 7.4 occurred on the North Anatolian Fault Zone with a macroseismic epicenter near the town of Golcuk in the western part of Turkey. Figure 2.3.1 illustrates the ruptured fault segments and the fault slip distribution model associated with this earthquake (Erdik, 2000). The total observable length of the rupture was about 100km. The lateral offset varied between 1.5 and 5m. Most of the aftershock activity is confined to the region bounded by 40.5-40.8N and 29.8-30.0E, which covers the area between Izmit and Adapazari to the east of the epicenter.

2.3.1. Ground Motion

The strong motion stations operated by the General Directorate of Disaster Affairs, the Kandilli Observatory and Earthquake Research Institute of Bogazici University and Istanbul Technical University have produced at least 27 strong motion records for the Kocaeli earthquake within 200 km of the fault. Kocaeli earthquake has generated six motions within 20 km of the fault (Sakarya, Yarimca, Izmit, Duzce, Arcelik, and Gebze), adding significantly to the near-field database of ground motions for Mw >= 7.0 strike-slip earthquakes. The peak ground accelerations recorded at the near fault stations in earthquake are provided in Figure 2.3.2. The two stations closest to the fault rupture are Sakarya (3.3 km) and Yarimca (4.4 km). Sakarya is founded on stiff soil, while Yarimca is founded on soft soil. Of these, the largest peak ground acceleration was about 0.4g at Sakarya. All of the attenuation relationships over predict peak accelerations observed in Kocaeli earthquake at distances less than about 20 km. However the peak velocities is in the order of what has been observed in previous earthquakes of similar nature. As it has been observed in almost all past earthquakes, the ground motion amplitudes are larger for the soil sites (Yarimca, Düzce) than for the rock sites (Gebze, Izmit, Sakarya)

The Duzce (DZC) record is the only record closer than 20 km that falls above the median prediction. This record was affected by rupture directivity. The Ambarli (ATS) site recorded unusually large accelerations (above the plus two standard deviation prediction for each attenuation relationship), possibly due to strong focusing and site effects. In Kocaeli earthquake the fault ruptured from Golcuk first to the west approximately 40 km then rupturing approximately 80 km to the east. Forward directivity may be observed both to the east and west of the fault. The western segment of the August 17 fault ruptured from east to west in the Izmit Bay for an unknown distance. As indicated in the source rupture models developed for the earthquake, the directivity effects may have contributed to damage in Yalova. And Cinarcik. Forward directivity can be observed both to the east and west of the fault. Sakarya and Yarimca records display strong velocity pulses and a static displacement of 2.0 m and 1.5 m, respectively, in the E-W component. The N-S component of the Yarimca (YPT) record also displays a significant static offset (1.2 m), indicating some movement to the north. Yarimca record is rather complex compared to others and clearly indicates an early aftershock with high frequency vibrations originating very close to the main shock epicenter. The complexity of the waveform at YPT may also indicate the influence of the local geology at the site. At Arcelik (ARC) the waveform is simple. The largest motion is in fault normal direction with the peak amplitude directed towards south. At Sakarya record (SKR) the time difference between the s- and p- wave arrivals is only 1.8s. This may be taken as an indication

that the rupture might have propagated at a supershear velocity of 4.7km/s between the source and the SKR station.

2.3.2. Damage Distribution

The damage caused by the earthquake covered a very large region extending from Tekirdag to Eskisehir, cities mostly affected being, Sakarya, Yalova, Kocaeli, Bolu and Istanbul. The intensively damaged region follows an area of about 20km wide (10km to the north and south of the fault) along the fault rupture. The number of condemned buildings after the earthquakes amounted 23,400. About 16,400 of these were heavily damaged and collapsed buildings during the earthquakes, which encompasses around 93,000 housing units and 15,000 small business units. Another 220,000 housing units and 21,000 small business units have experienced lesser degrees of damage. As much as 120,000 families were left in need of homes after the earthquake. The number totally collapsed buildings (pancake collapse) is estimated to be in the range of 3,000-3,500. There were 18,373 accounted deaths and 48,901 hospitalized injuries. The general isoseismal map of this earthquake is provided in Figure 2.3.3 (after, General Directorate of Disaster Affairs). As it can be seen in Istanbul the general intensity is VI with a limited region of intensity VII in the Avcilar area to the west of Istanbul. The damage distribution in Istanbul as a result of the Kocaeli earthquake is provided in Figure 2.3.4 after the Governor's Office of Istanbul. Figure 2.3.5 through Figure 2.3.7 illustrate the distributions of moderately, heavily and totally damaged buildings in Istanbul. The damaged area is also indicated in Figure 2.3.8 (after earthquake and Soils Directorate of Istanbul Metropolitan Municipality). This earthquake is associated with fault segments 1,2,3, and 4 (Figure 2.2.13) (Erdik (2000), Ambraseys (2000), Hubert-Ferrari et al. (2000)).

Following damages are reported in the Province of Istanbul (After, Governorate of Istanbul, Disaster Management Center, Briefing 2002 Power Point Files)

Damaged (light to collapse) number of residential business units in Istanbul: 41,180
Damaged (light to collapse) number of public buildings in Istanbul: 1,545 (about 11% of the total number of public buildings, cost of repair and retrofit is estimated to be about 100 Million USD)
Damaged (light to collapse) number of schools in Istanbul: 820
Number of families temporarily housed: 18,162
Number of totally collapsed (pancake collapse) buildings: 81

2.3.3. Effects in Avcilar

Avcilar, to the west of Istanbul, exhibited relatively high rates of building damage as it can be assessed from Figure 2.3.9. The distribution building damage in the Avcilar area, as illustrated in Figure 2.3.9, is as follows:

Totally Collapsed: 28
Heavy Damaged Buildings: 86
Medium Damaged Buildings: 501
Light Damaged Buildings: 801
Total Number of Buildings: 17863

Assuming similar average building conditions throughout the Istanbul region, the relatively high damage logically translates to relatively high earthquake ground motions experienced in the 1999 Kocaeli earthquake, which is evidenced by strong motion records with high peak accelerations in surrounding areas of Cekmece and Ambarli (Erdik, 2000). For this

earthquake, such relatively high ground motions can be manifestations of either propagation path effects or local site effects.

Site effects at Avcılar were estimated using S waves from both types of records (Ozel et.al, 2000). The results show that the amplifying frequency band is, in general, lower than 4 Hz and the geology of the area is capable of amplifying the motions by a factor of 5-10. In this frequency band, there is a good agreement between the spectral ratios from the two main shocks and their aftershocks. Kudo et.al (2000) has shown that the large and long duration of strong motion records at Ambarli (ATS) are closely related to the low velocity (Vs~200m/s) of surface layers. The S-wave velocity structure at Avcılar is similar to the lowland Ambarli (ATS) and the strong ground motion at Avcılar during the mainshock is estimated to be similar to that at ATS.

After the 1999 Kocaeli earthquake a five-station special strong motion array was placed in the Avcılar area by KOERI of Bogazici University for the determination of site-specific effects on the earthquake ground motion (Ozbey, 2002). When the time domain characteristics of ground motion obtained at the station ATS (Ambarli) and five temporary stations were examined, it is assessed that the ATS station can be accepted as a representative station for Avcılar district. Time and frequency domain comparison of all acceleration records obtained at the station ATS were compared with the other stations close to it no but no evidence of amplification was observed. Further investigation was carried out to examine the variation of motion with azimuth, but again it was seen that the ground motions characteristics did not show significant variation with azimuth. Thus it would be difficult to explain the relatively heavy damage at Avcılar during 1999 Kocaeli Earthquake by site amplification only. The reason for this may be what is called Crustal Waveguide Effects (Moho Effect). At close distances (R<50km) the largest ground motions are caused by waves that travel upward from the earthquake source to the site. As distance from the source increases the reflections of down going waves from interfaces below the source reach the critical angle and undergo total internal reflection. This is called Crustal Waveguide Effect, and cause damage at sites with fault distances of range 60-100km. Similar incidences of "Moho Effect" has also been observed in Loma Prieta earthquake (Somerville, 1990). Fault distance of Avcılar at the Kocaeli Earthquake was 80 km. This might be the reason for the heavy damage experienced in Avcılar during the Kocaeli Earthquake but it still needs to be examined in detail.
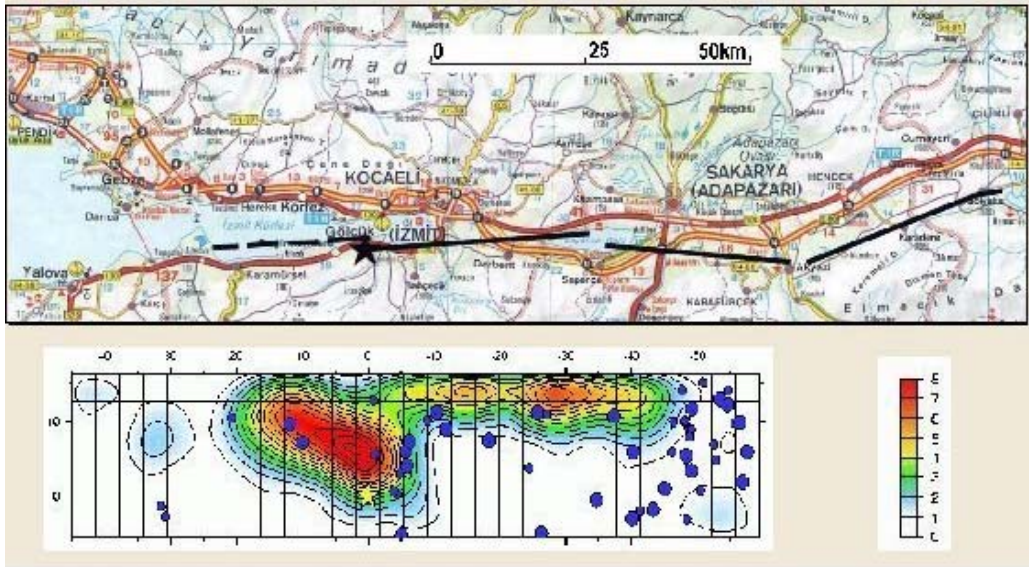
Figure 2.3.1. Surface fault ruptures and slip model of the August 17, 1999 Kocaeli earthquake (Erdik, 2000).

Figure 2.3.2. Peak horizontal ground accelerations recorded in the Kocaeli earthquake.
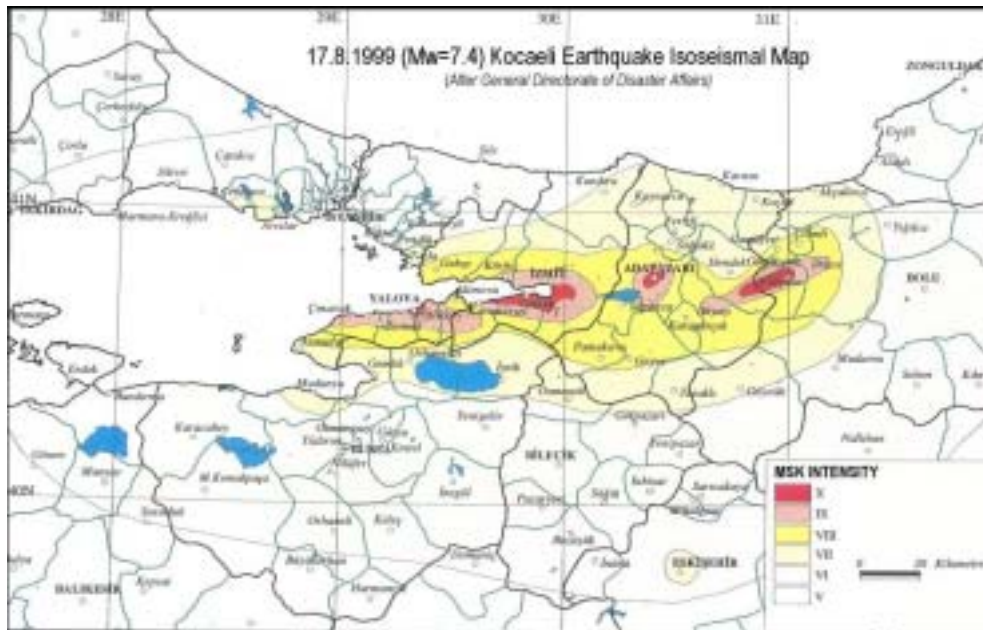
Figure 2.3.3. Iso-seismal map of August 17, 1999 Kocaeli earthquake (After B.Ozmen of Gen.Dir. of Disaster Affairs).
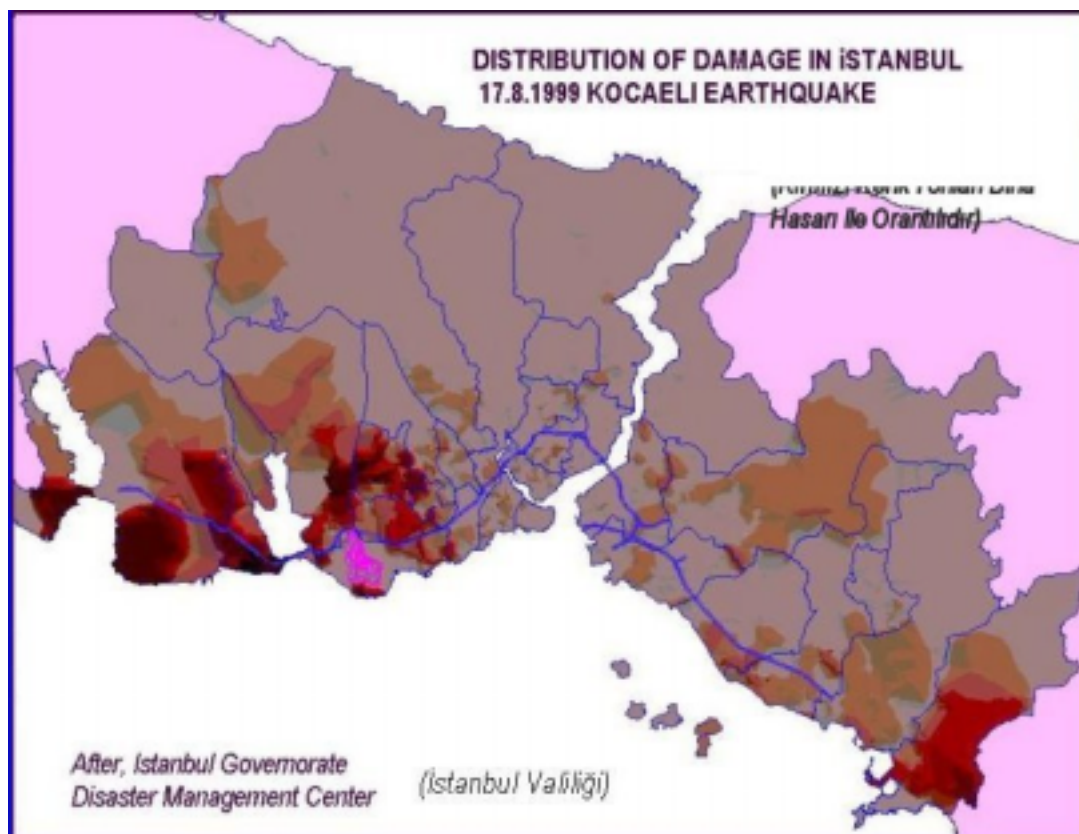
Figure 2.3.4. Distribution of damage in Istanbul due to August 17, 1999 Kocaeli earthquake.
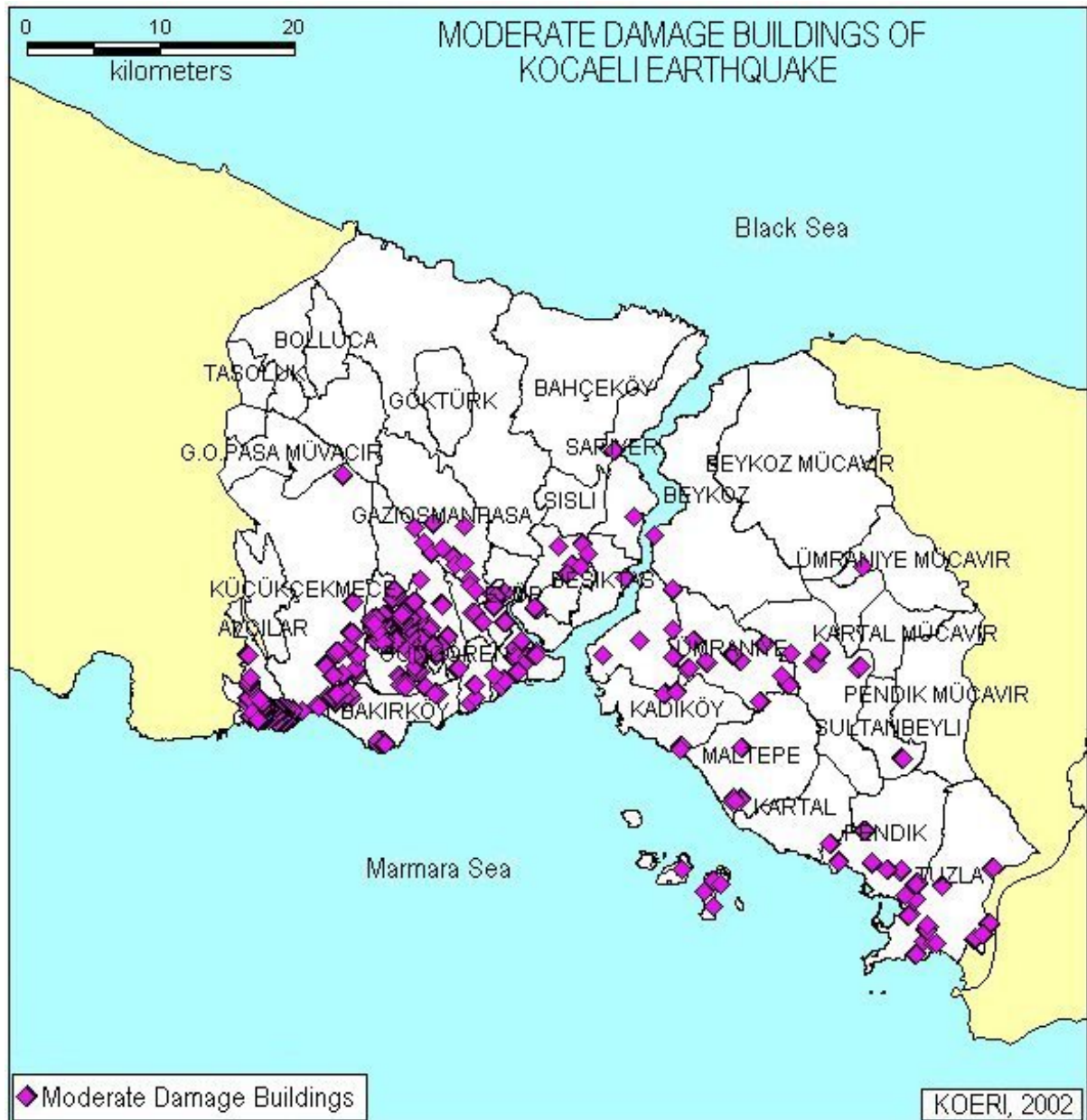
Figure 2.3.5. Distribution of moderate damaged buildings in Istanbul due to August 17, 1999 Kocaeli earthquake.

Figure 2.3.6. Distribution of heavy damaged buildings in Istanbul due to August 17, 1999 Kocaeli earthquake.

Figure 2.3.7. Distribution of totally collapsed buildings in Istanbul due to August 17, 1999 Kocaeli earthquake.
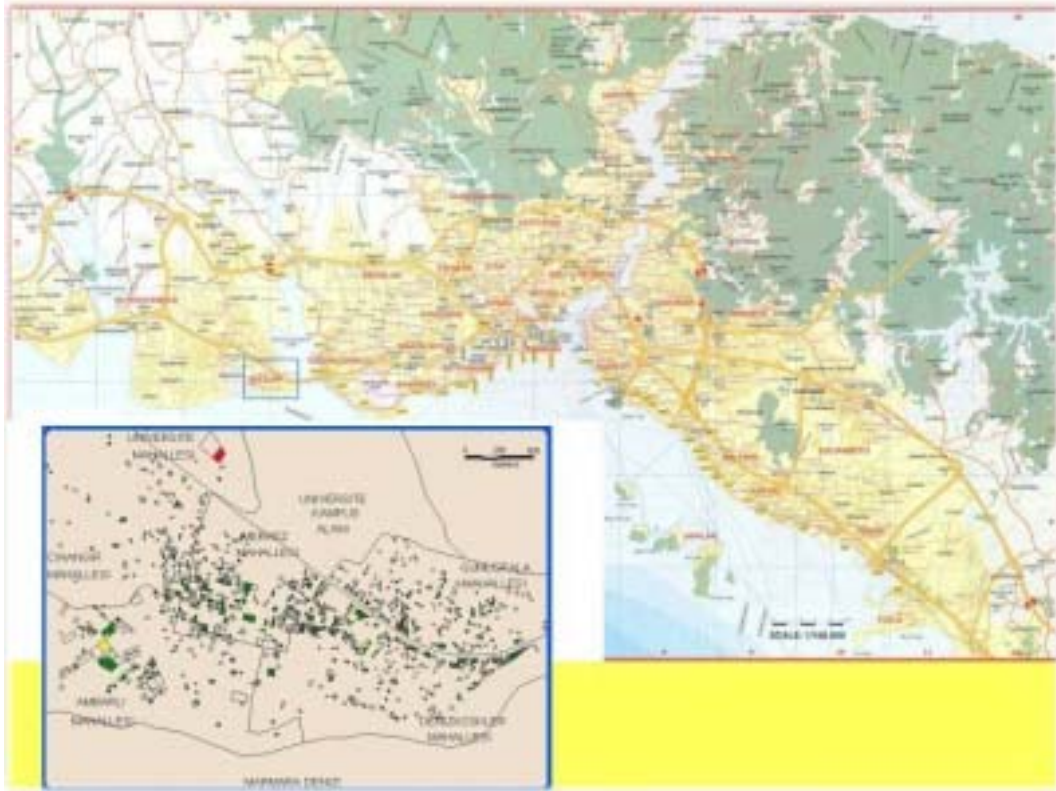
Figure 2.3.8. Damage occurred in Avcilar due to August 17, 1999 Kocaeli earthquake.
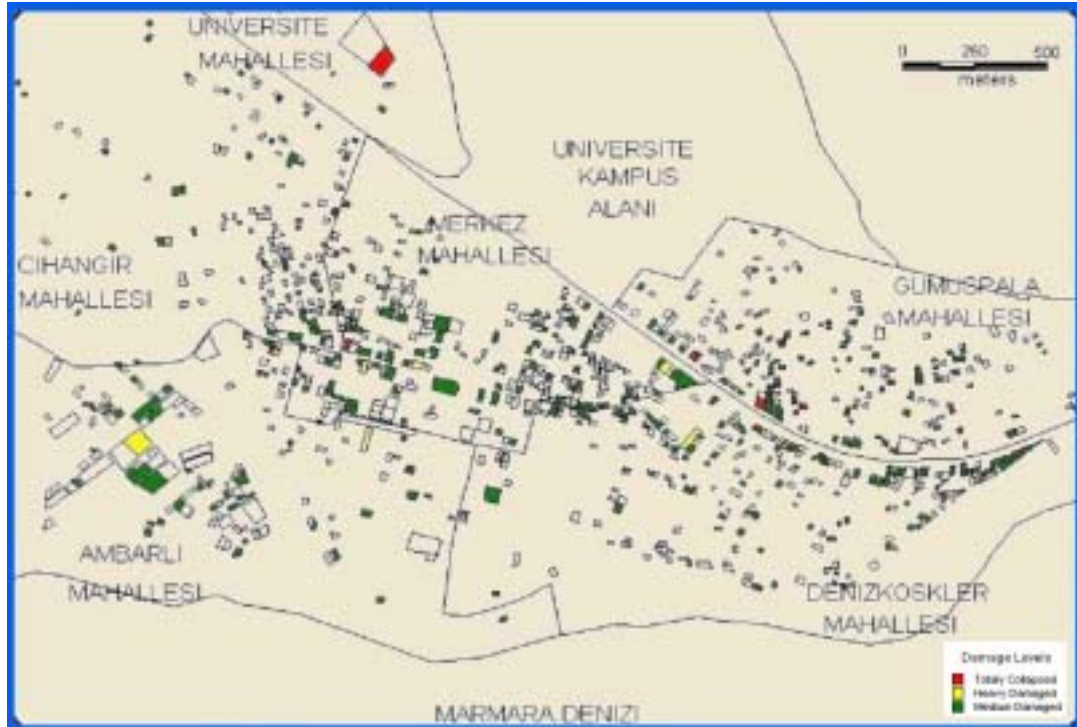
Figure 2.3.9. Damage Distribution in Avcilar.

2.4. GEOLOGIC AND GEOTECHNICAL CONDITIONS IN ISTANBUL

2.4.1. Geographic Structure in Istanbul

Istanbul is characterized by a number of significant topographical features. The most prominent one is the Bosphorus, a narrow strip of water, which forms a portion of dividing line between continents of Europe and Asia and divides the city of Istanbul. On the European side are the Golden Horn, a remarkable natural harbor; the Buyukcekmece and Kucukcekmece Lakes or lagoons; a continuous succession of low rolling hills which form a number of major and minor drainage basins flowing either to the Sea of Marmara, the Golden Horn or the Bosphorus (Figure 2.4.1). Two major of streams, Kagithane and Alibey, flow into the Golden Horn. Along the Marmara coast west of the Golden Horn, a plateau with shallow valleys running north and south generally perpendicular to the coastline. The highest point in Istanbul is Buyuk Camlica with an elevation of 250m. As in European side of Istanbul the areas along the Bosphorus have steep banks, but those along the Sea of Marmara are more gradual in profile. The Asian side, has a greater variety of physical features. Easterly beyond the steep banks of the Bosphorus, the terrain varies from very hilly to mountainous. Istanbul is a city of many hills, with relatively flat areas, slightly above sea level, along the shores of the Bosphorus, the Golden Horn and the Sea of Marmara. The flat areas vary from a simple road width, as in many cases along the Bosphorus., to relatively wide strips typified along the Sea of Marmara in western Istanbul. The areas located along the Sea of Marmara do not rise as sharply as along the Bosphorus where coastline is quite steep and is cut by sharp narrow valleys. Slopes of 20 percent are common in these areas. The Prince Islands are located approximately 7 km offshore from Asian side of Istanbul in the Sea of Marmara. The shoreline of the islands is generally very steep (Figure 2.4.2).The Bosphorus is a meandering strait about 31km in length with an average depth of 35m.

2.4.2. Geology of Istanbul and Vicinity

The surface geology map with a scale of 1/50,000 prepared by Istanbul Metropolitan Municipality is shown Figure 2.4.3 and Figure 2.4.4. As it can be seen from Figure, the northern, northeastern and central parts of Istanbul are dominated by Paleozoic shale and greywacke. Various folds, faults, fractures and joint sets have been identified in this formation, mainly due to two orogenic episodes, the Hertcynian and the Alpine, which significantly affected this area. The southern part of Asia side of the city are dominated several formations such as Kurtköy, Gozdag, Aydos, Tuzla, Kartal and Dolayoba formations. The late Ordovisian, Kurtköy formation includes purple-red brown fine to course grained generally medium to thickly bedded sandstone, moderately strong to strong. It is mostly highly weathered. Generally the formation has a deep weathering profile. Aydos formation is composed of pink and light yellow, fine-grained medium to thickly bedded moderately widely to widely jointed quartzitic sandstone, strong to extremely strong. This unit generally forms high ridges in places. Gozdag formation (the middle Devonian) are a fine to medium grained feldspathic sandstone (greywacke), weak to moderately strong and a fine-grained laminated to thinly bedded mudstone/shale, moderately weak to weak. Dolayoba formation comprises a light gray and blue gray massive coralline/fossilifereous limestone, strong, and dark blue grey, fine to medium grained medium bedded calcareous shale, moderately weak to moderately strong. The middle Devonian, Kartal formation is composed of a brown and gray brown thinly to medium bedded very fossilifereous shale/mudstone, moderately weak to moderately strong, alternating with a fine to coarse-grained medium bedded sandy limestone, moderately strong to strong. Tuzla formation mainly consists of light gray thinly to medium

bedded nodular/muddy limestone, moderately strong to strong, interbedded with gray thinly bedded to laminated calcareous shales with high silicium content. The Paleozoic basement consists of upper Devonian, Trakya formation interbedded medium to fine-grained sandstone, siltstone, greywacke and micaceous shale. It consists of brown and yellow, when highly weathered, and green gray and gray when fresh, fine to coarse grained medium to thickly bedded feldspathic sandstone, moderately strong to strong, alternating with brown green gray thinly to medium bedded, siltstone/mudstone. These rock units are easily weathered by the effect of surface waters. Baltalimanı formation (upper Devonian) comprises a dark brown gray black very thinly bedded phoshatic nodular chert-lydite, very strong, being tightly folded due to syngenetic slides.

The northern of the city are dominated by Mesozoic basement discomformably overlie Paleozoic strata such as Sariyer formation contains marl, mudstone and Karaburun-Cukurcesme formation unweathered including marl, coal, clay and tuff mixtures. The Tertiary sediments and rocks lie directly on the top of the Paleozoic Peneplain surface, indicating a long period of interruption of deposition and/or erosion of the latter in the stratigraphic record. The Tertiary formations nearest to the Golden Horn are found within the walled part of the old city. The middle Eocene, Ceylan formation consists of marls interbedded with bedded limestones and mudstones, light gray blue and gray medium bedded to massive sandy marl, brown light gray fine grained medium bedded. Sogucak formation including of reef limestone, partly dolomitized and detrial limestone, gray to yellow brown, fine-grained, medium bedded, moderately strong to strong. The Oligocene, Gurpinar formation extends around Buyukcekmece and Kucukcekmece Lakes at the southern part of Istanbul. This formation consists of alternating layers of gravel and gravelly silty clayey sand, clay, marl, tuff-tuffit, claystone, sandstone. It is named as Karaburun formation in the northern coast of Istanbul. The coastal region between Catalca and the Bosphorous consist of to lagoonal sedimentary rocks. This stratum lays unconformly over the Eocene shelly limestones and Paleozoic rocks extending to the Prince Islands.

The upper Miocene sediments and sedimentary rocks (Cukurcesme, Gungoren and Bakirkoy formations) including sand and gravel, clay and marl, and limestone extend over the Paleozoic basement. Upper Miocene, Cukurcesme formation contains yellowish-brown-beige, dense to very dense sand, silty sand, clayey sand, gravel and clay. Gungoren formation is formed greenish-gray clay fissured, highly plastic thin laminated clays, with thin peat layers and sand-silt levels. Bakirkoy formation in the south part of the city is comprised of white, porous, chalky, medium to hard limestone with clay interbeds, typically thick-bedded and fine-grained. This formation comprises a cream to greenish yellow fine-grained medium to thickly bedded closely jointed moderately limestone and marl interbedded with greenish cream highly plastic shelly hard clay.

The Quaternary, Kusdili formation (marine quaternary) consists of overconsolidated clay, sand and mud. This deposit is come across southern coast of Küçükçekmece Lake and in the Golden Horn. The Quaternary deposits and natural fills consist primarily of loose to very loose, medium to fine silty, shelly sand and dark gray clay and mud. Recent alluvium deposits as river sediments comprise gravel, sand and clay. Alibey and Kagithane rivers transported large amounts of erosion material into the Golden Horn. Alluvium can be encountered in creek valleys and plains in the study area. The recent manmade fill is dominated along the south coast of Asia side. This artificial fill consists of dense, course to fine sand and gravel mixed silt, clay, and cobbles.

2.4.3. Geotechnical Conditions

For this purpose, any special site investigations (drilling, PS logging and microtremor) have not been carried out. However data utilized for this purpose has been obtained from available studies, which were conducted before different surveys in Istanbul. We evaluated approximately 300 borehole investigations and 50 PS logging and 40 microtremor studies.

2.4.4. NEHRP Site Classes

The basic approach towards the assessment of the spatial variation of geotechnical conditions includes the determination the soil classes to be used. For this purpose we have adopted the NEHRP (1997) soil classification. This classification has international acceptance in earthquake engineering profession and will facilitate the differentiation of ground motion (i.e. site response or site amplification) with respect to different site classes.

The NEHRP (1997) Site classes are defined as follows:
   A Class: Hard rock with measured shear wave velocity Vs>1500 m/s
   B Class: Rock with (760 m/s< Vs<1500 m/s)
   C Class: Very dense soil and rock with (360 m/s<Vs<760 m/s) or with either Standard
      Penetration Resistance N>50 or Average Undrained Shear Strength at top 30 m
      Su>=100 kPa
   D Class: Stiff soil with (180 m/s<Vs<360 m/s) or with either 15<N<50 or (50
      kPa<Su<100 kPa)
   E Class: A soil profile with Vs<180 m/s or with PI>20 and Su<25 kPa
   F Class: Soils requiring site-specific evaluations:
      1. Soils vulnerable to potential or collapse under seismic loading such as
         liquefiable soils quick and highly sensitive clays, collapsible weakly cemented
         soils
      2. Peat and/or highly organic clays with thickness H>3 m of peat and/or highly
         organic clay
      3. Very high plasticity clays (H>8 m with PI>75)
      4. Very thick soft/medium stiff clays (H>36 m)

The spatial distribution of these soil classes in Istanbul (Soil Classification Map of Istanbul) was developed and first presented in the Interim Report-1. This Figure is essentially based on the information obtained from the 1/50,000 scale surface geology map prepared by Istanbul Metropolitan Municipality and limited borehole data obtained from the 17th Division of the Turkish State Highways. Geological information provided in this map has been interpreted. This information provided by the "Soil Classification Map of Istanbul" in terms of NEHRP (1997) soil classifications will be used for the site-specific modification of the earthquake ground motion.

The updated "Soil Classification Map of Istanbul" which is illustrated in Figure 2.4.5 has been formed by taking into consideration about 300 boreholes data and carried out at different places entire Istanbul. We would like to express thanks for data bank of Zetas Geotechnical and Foundation Investigations Co.
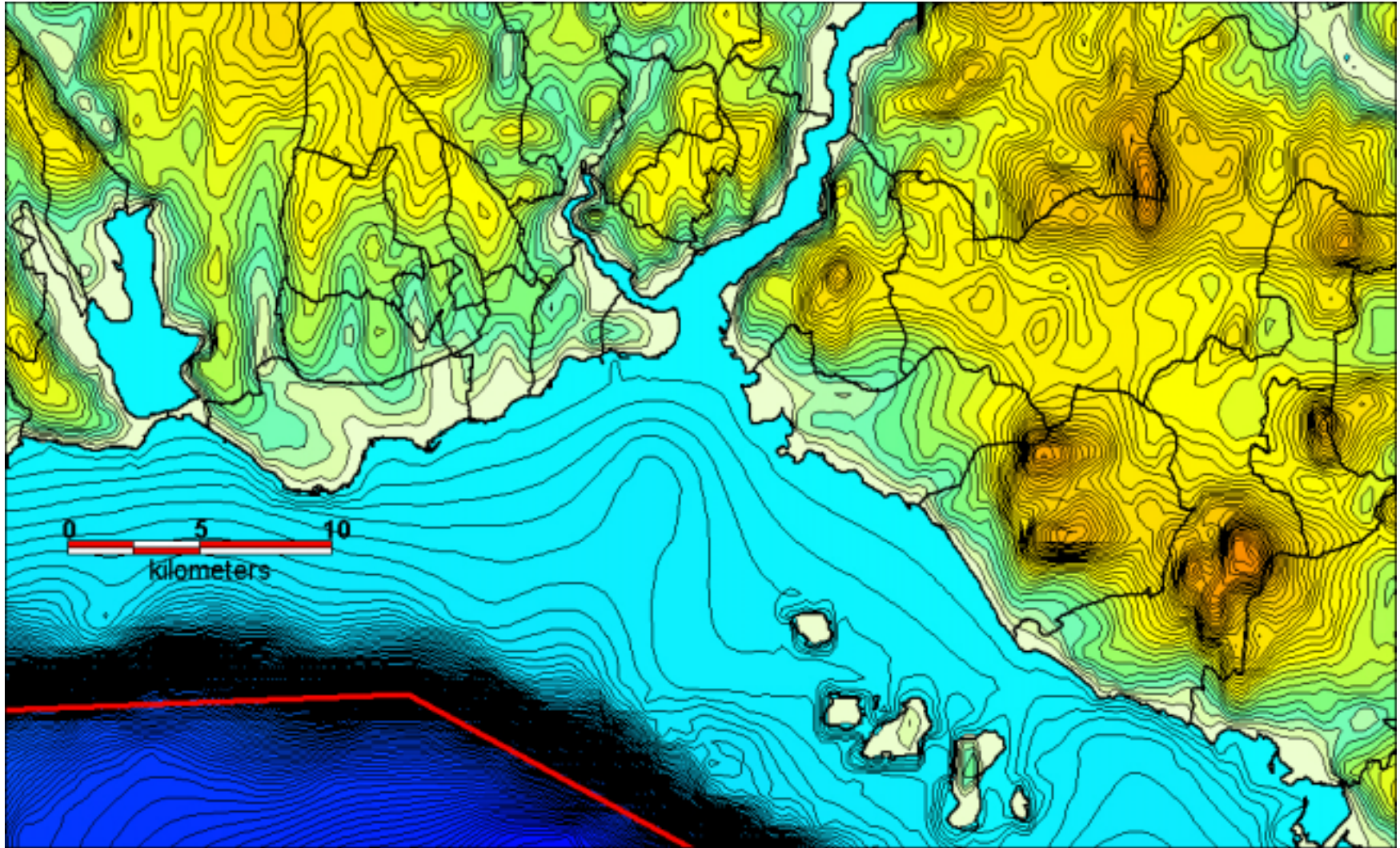
Figure 2.4.1. General topographic map of the region combined with bathymetry.
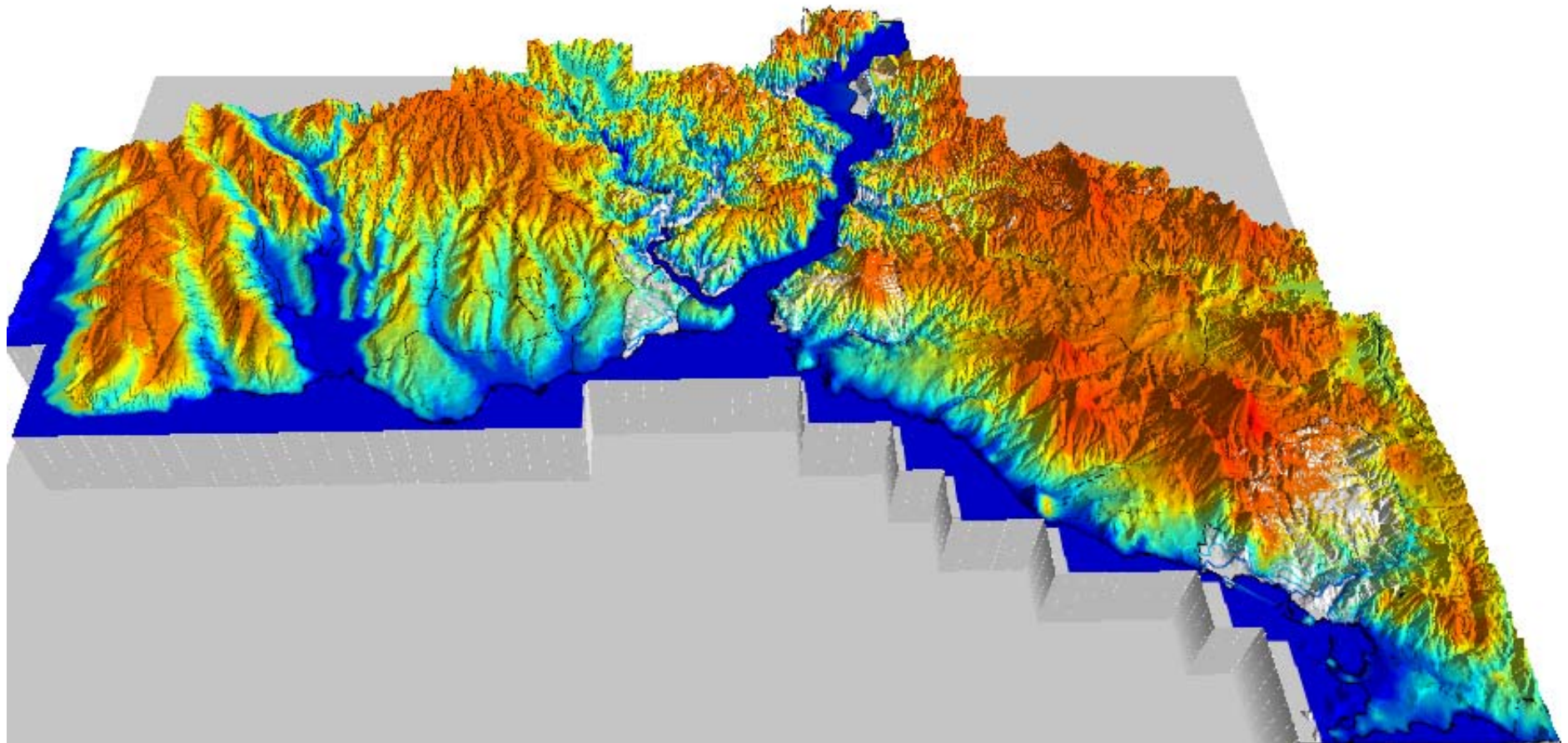
Figure 2.4.2. 3D topographic map of the region.
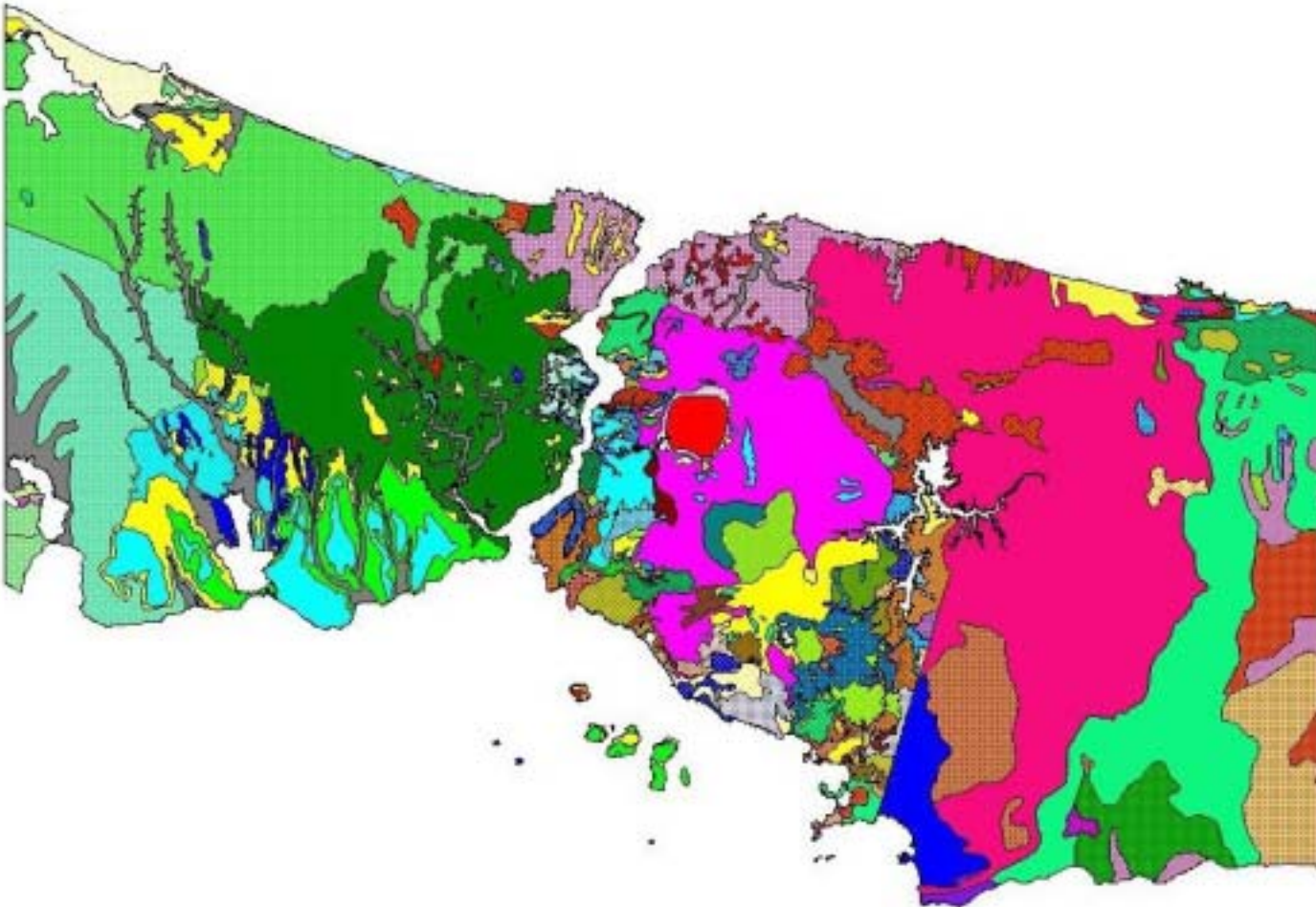
Figure 2.4.3. The surface geology map of Istanbul (After Istanbul Metropolitan Municipality).
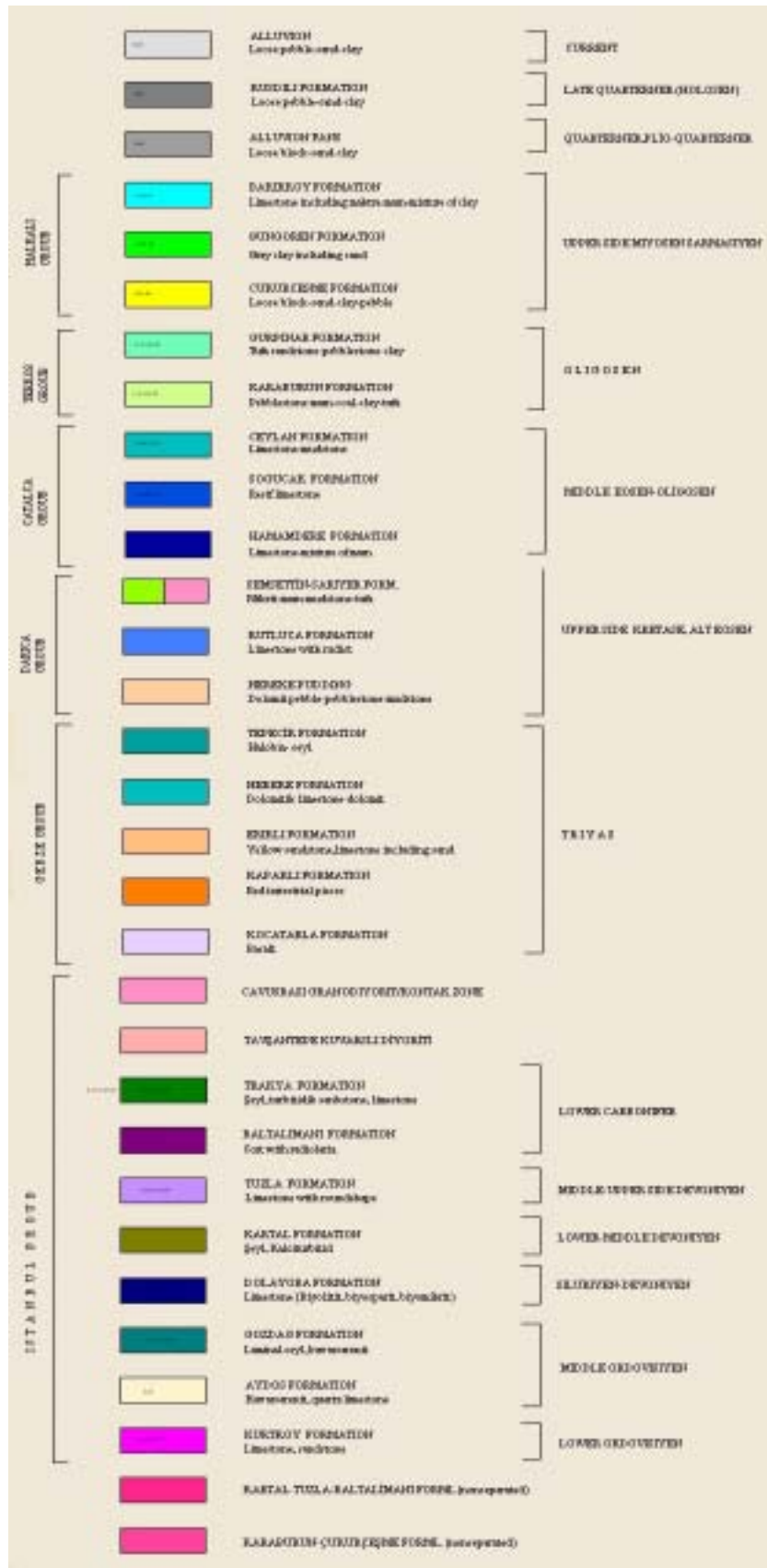
Figure 2.4.4. Legend for the surface geology map of Istanbul (After Istanbul Metropolitan Municipality).
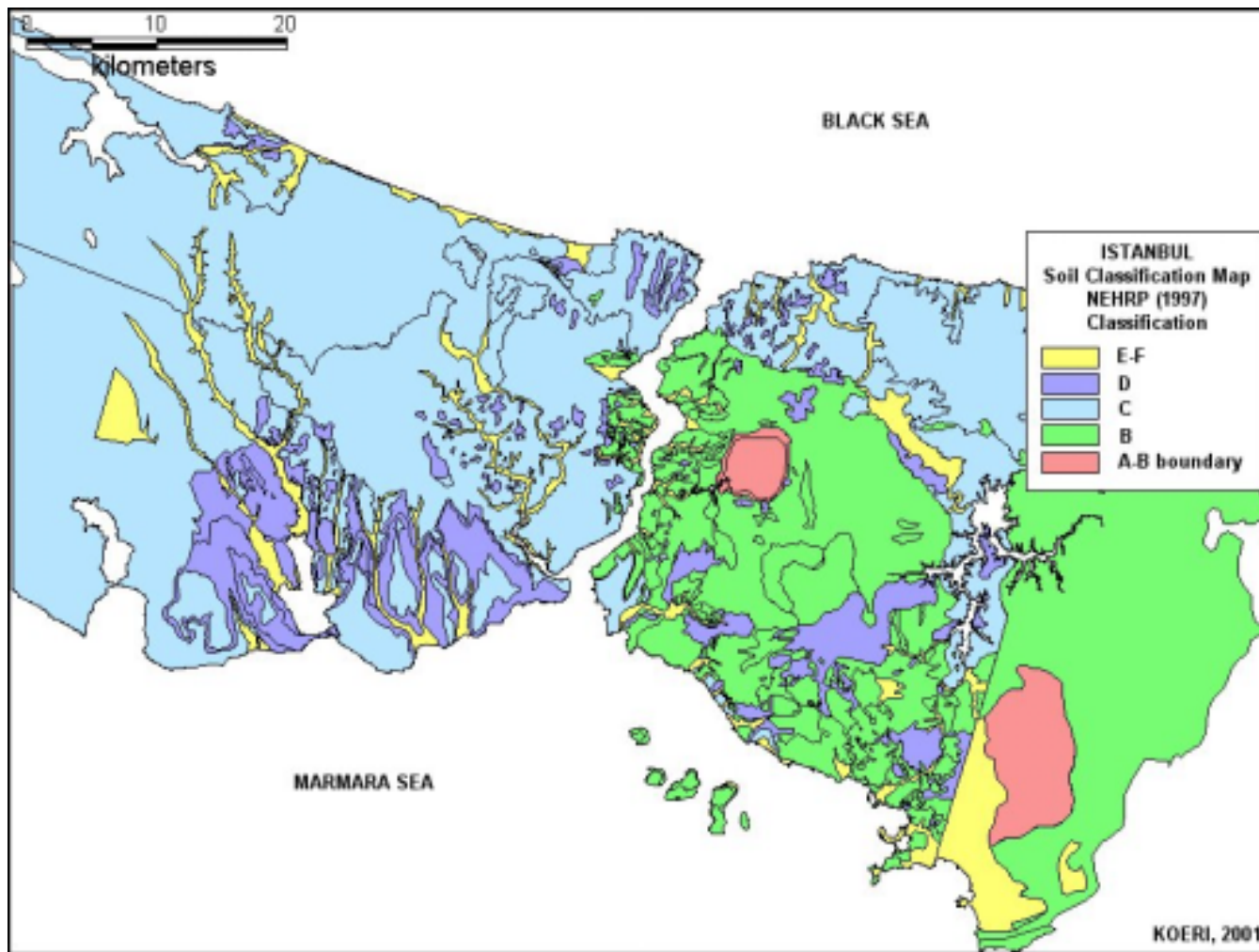
Figure 2.4.5. The NEHRP-based Soil Classification Map of Istanbul.

2.5. EARTHQUAKE GROUND MOTION

2.5.1. General Approaches

Topics associated with the evaluation (probabilistic or deterministic) of ground motion involves consideration of:

- Earthquake Source Process
- De-aggregation of Probabilistic Hazard
- Empirical Attenuation Relationships
- Near Fault Effects (Radiation Pattern and Directivity)
- Site Response
- Analytical Simulation Procedures

The elastic rebound theory proposed by Reid in 1911 constitutes the essential foundation of the earthquake source process used in the modeling of strong ground motion. The sudden fault rupture that results from the accumulation of strains in the crust, is the cause for the radiation of seismic waves and, consequently, of the ground motion. The development and the propagation of the dislocation front on the fault surface and the time for the completion of the slip are essential for the explanation of the ground motion. Seismic moment, various stress parameters, rupture velocity and slip time functions are considered as the main parameters needed for description of the source and for the simulation of ground motion. It has been repeatedly shown that the strong motion acceleration time history is highly influenced by the complexity of the source rupture due to fault heterogeneities. Thus a proper description of the source process, especially in connection with the scenario earthquake (or de-aggregated source event), is important for the simulation of ground motion for any site or, spatially, in a given urban area.

Empirical attenuation relationships, covered in detail in Chapter 2.5.2, are generally employed in the quantification of seismic hazard in either deterministic or probabilistic approaches. These attenuation relationships exist for Intensity, PGA, PGV, Arias Intensity, duration related parameters and Spectral Accelerations. All empirical attenuation relationships are based on or calibrated against strong motion databases.

Attenuation models provide for the change of ground motion severity with source mechanism, distance and local geology. Currently reliable empirical models exist in terms of peak ground acceleration, velocity and displacement (PGA, PGV and PGD) and, pseudo spectral velocity (PSV), at specific frequencies and damping ratios, for given earthquake magnitude, distance, fault mechanism and local geology. Although the data are biased towards well-instrumented regions of the world, recent comparisons indicate that, with identical definitions of input parameters, the difference amongst Western USA, Japanese and European based attenuation relationships are less than the scatter in any one of them. This finding enhances their utilization in other parts of the world with limited strong motion data. The availability of intensity-based vulnerability information has dictated the use of site-specific intensity attenuation relationships. These relationships are based on macroseismic data obtained from past earthquakes and yield MM, MSK or JMA intensities for given earthquake magnitude, distance and, possibly, for site conditions and fault mechanism. Owing to the subjective nature of the intensity scales, in most cases they are associated with substantial uncertainties reaching 0.6 MM units.

Strong ground motion attenuation relationships may provide ground motion estimates for sites with typified soil conditions (Such as NEHRP Soil Classes) of for given values of average shear wave propagation velocity in the upper 30m of the soil medium. Generally one-dimensional non-linear (or equivalent linear) site response analysis is used for the assessment of the potential of site amplification of soil failure (i.e. liquefaction or landslide) at susceptible sites (such as NEHRP Site Class F). Although variations in ground motion can occur in association with highly irregular (ridge or canyon) topographies and deep basins, such pronounced topographies do not generally exist in the Istanbul urban region.

The amplitude and polarity of a seismic wave radiated from an earthquake source change with the orientation of the source and the receiver. This dependence is called as the radiation pattern. There is a difference in the radiation patterns of P and S waves for a point source For a rupture propagating at a certain velocity along a fault plane, stations located in the direction of rupture propagation experience shorter duration ground motions than the ones located in the direction opposite to the direction of rupture. This is called directivity. Associated ground motion amplitudes are larger for stations in the forward directivity region than the ones in backward directivity region due to conservation of energy. At high period ranges forward directivity effects at near-fault locations result in high amplitude velocity pulses. The fault normal component of the ground velocity will generally consist of a full cycle velocity pulse, which upon integration will not create a permanent displacement. Whereas, the fault parallel components will generally have half-cycle velocity pulse, which creates a permanent absolute displacement equal to the fault offset. The directivity effects can be routinely incorporated in the deterministic hazard assessments. Considering the geometry of the fault rupture in the scenario earthquake considered for Istanbul (Chapter 2.7.1), we could investigate the possible effects of directivity using Somerville et al. (1997) methodology. For a total fault rupture length of about 120km and an average distance of 20km to urban Istanbul the directivity effects will be minimal for an earthquake origination in the middle of the fault area and propagating bi-directionally. However significant directivity effects can be observed in the regions located at the opposite end of the fault rupture for the earthquake that starts to rupture at the other end and ruptures uni-directionally. In this case, for a general building stock, where the natural period of vibration does not exceed 1s, the directivity effect will manifest itself with a less than 20% increase in the spectral accelerations for period 1s, decreasing gradually to %0 at the period 0.7s.

2.5.2. Attenuation Relationships

The limited strong motion data in Turkey and also in the Eastern Mediterranean region and ambiguities on the station site descriptions does not allow for the development of reliable region and site specific development of ground motion attenuation relationships. However Ozbey (2001) recently has developed an attenuation relationship for PGA applicable to Northwestern Turkey using a data set consisting of Kocaeli and Duzce earthquake main- and aftershock records mainly.

Owing to the geological and geo-tectonic similarity of Anatolia to the California (Strike slip faults similar to North and East Anatolian Faults) and also on the basis of favorable predictive comparisons it is decided to be rational and prudent to utilize, the following attenuation relationships currently being used for the assessment of earthquake hazard for the Western US (Leyendecker et. al., 2000)

For Peak Ground Acceleration (PGA): Boore, Joyner and Fumal (1997), Sadigh et. al.(1997), Campbell (1997) and Ozbey (2001) relationships will be utilized. The average of Boore, Joyner and Fumal (1997), Sadigh et. al.(1997) and Campbell (1997) will used in the assessment of distribution of peak ground acceleration in the region. The result of will be compared with the results of the Ozbey (2001) relationship, which is produced based on data from the Kocaeli and Duzce earthquakes.

For Spectral Acceleration (SA), following Leyendecker et. al.(2000) the average of Boore, Joyner and Fumal (1997) and Sadigh et.al.(1997) will be utilized.

Region specific intensity attenuation relationships developed on the basis of Anatolian earthquakes Erdik et.al, (1985) will be considered for the assessment of seismic hazard on the basis of MSK intensities. For the applicability of this attenuation relationship for Istanbul, see Figure 2.3.3 where its comparison with the iso-seismal map of the Kocaeli earthquake is provided.

Details of the attenuation relationships named above are provided in Appendix 2.

2.6. PROBABILISTIC EARTHQUAKE HAZARD

2.6.1. Earthquake Data Base

The earthquake catalog compiled for the Assessment of Earthquake Hazard in Turkey and Neighboring Regions as a cooperative project of GSHAP (Global Seismic Hazard Program) (Erdik et al.,1999) has been used for this study. The earthquake catalog has been compiled from various catalogs of historical and instrumental seismicity of the region and comprised events with magnitude M>5.5. CNSS catalog has been used for the events of the 20th century with magnitude between 5.0 and 5.5, and CNSS and KOERI catalogs have been used for the compilation of the events with magnitude 4.5-5.0 occurred in the last 35 years. To ensure the time and location independency of the events the whole catalog has been reviewed and fore- and aftershocks have been removed.

2.6.2. Earthquake Occurrence

For forecasting seismic occurrences numerous models have been developed. The simplest stochastic model for earthquake occurrences is the Homogeneous Poisson Model. For the earthquake events to follow that model, the following assumptions are in order:

1) Earthquakes are spatially independent;
2) Earthquakes are temporally independent;
3) Probability that two seismic events will take place at the same time and at the same place approaches zero.

Obviously the above assumptions are difficult to justify for the Marmara region, due to the domino effect rupture propagation and the known seismic gaps in the North Anatolian Fault and the change in the stress regime as the result of the 1999 earthquakes.

2.6.3. Conditional Probability (Renewal) Model

The relationship between the fault geometry and the slip variation along the North Anatolian Fault strongly indicate a "segmentation" behavior analogous to the San Andreas Fault in California (Barka, 1996). The characteristic earthquake hypothesis is based on the premise that the slip is dominated by earthquakes that rupture the entire segment with a characteristic displacement. For the Marmara segmentation scheme that we have developed in this study (Figure 2.2.13), we presumed that segment boundaries exist where faults change direction, or where the displacement varied substantially in the past earthquakes. The associated median recurrence times for the segments of the Northern Portion of the North Anatolian Fault in the Marmara Sea Region are provided in

Table 2.6.1, based on our best estimates in consideration of the past seismic activity elaborated in Section 2.2.1.1 and illustrated in Figure 2.2.20 through Figure 2.2.24.

Table 2.6.1. Fault segmentation, associated median recurrence times and annual rates of occurrence for the northern portion of the North Anatolian Fault in the Marmara Sea region.

Fault Segment	Last Earthquake	Median Recurrence Time, m	Annual Rate of Occurrence, r
1	12.11.1999(Mw=7.1, Ms=7.3)		
2	17.8.1999 (Mw=7.4, Ms=7.8)	140 ± 35 years*	7.14*10⁻³
3	17.8.1999 (Mw=7.4, Ms=7.8)	140 ± 35 years	7.14*10⁻³
4	17.8.1999 (Mw=7.4, Ms=7.8)	140 ± 35 years	7.14*10⁻³
5	10.7.1894 (Ms=7.3)	175 years	5.71*10⁻³
6	2.9.1754 (Ms=6.8)	210 ± 40 years*	4.76*10⁻³
7	22.5.1766 (Ms= 7.1)	250 years	4.00*10⁻³
8	22.5.1766 (Ms= 7.1)	250 years	4.00*10⁻³
9	10.5.1556 (Ms= 7.2)	200 ± 50 years*	5.00*10⁻³
10		200 ± 50 years*	5.00*10⁻³
11	9.8.1912 (Ms=7.3)	150 years	6.67*10⁻³

See Figure 2.2.20 *through* Figure 2.2.24 *for an illustration of historical earthquakes and associated segmentation, * estimated*

If we assume a homogenous Poisson process to model the occurrence of the characteristic earthquakes on each segment, the probability of having at least one (segment rupturing) characteristic earthquake on the segment within the time interval Δt is given by the following expression:

$$P[N \geq 1] = 1 - e^{-r.\Delta t} \qquad (2.1)$$

Where r is the annual rate of occurrence of the event, determined as the inverse of the median value of the recurrence time (m).

$$r = \frac{1}{m} \qquad (2.2)$$

Probability of the rupture of the segment (i.e. characteristic earthquake) in the time interval t_e, $t_e + \Delta t$ is given by (WGCEB, 1990) the following expression:

$$P(t_e \leq T \leq t_e + \Delta t) = \int_{t_e}^{t_e+\Delta t} f_T(t).dt \qquad (2.3)$$

Where t_e is the elapsed time since the last segment rupturing earthquake and $f_T(t)$ is the lognormal probability density function of the time of occurrence (T) of the segment rupturing (characteristic) earthquake.

$$f_T(t) = \frac{1}{t.s.\sqrt{2\pi}} . e^{-\left[\frac{\ln(t/m)^2}{2s^2} \right]} \qquad (2.4)$$

Where, m is the best median value of the recurrence interval T of the characteristic earthquake and s is the standard deviation of the natural logarithm of the time of occurrence (ln T). If S is not specifically known, it is generally assumed to be equal to one-third of ln (m).

The median value of the recurrence interval, m, can be determined from the ratio of the displacement (D) of the previous segment rupturing earthquakes and the best median estimate of the regional slip rate (V).

$$m = \frac{D}{V} \qquad (2.5)$$

For the Marmara sea the slip rate is found to be in the range of 2-3 cm/year (Armijo et. al, 1999)

The probability of occurrence of a segment-rupturing (characteristic) earthquake in the time interval t_e, $t_e + \Delta t$, given that the event did not happen prior to t_e, is given by the following expression:

$$P\left(t_e \leq T \leq t_e + \Delta t \middle| T > t_e\right) = \frac{P\left(t_e \leq T \leq t_e + \Delta t\right)}{P\left(t_e \leq T \leq \infty\right)} \qquad (2.6)$$

The nominator of this expression is equal to the hatched area, and the denominator is equal to the total blue colored area under the lognormal probability density function schematically drawn in Figure 2.6.10.

The lognormal distributions in the earthquake renewal models are characterized by the mean and the coefficient of variation. Assuming that it has been 200 years since the last earthquake on the Main Marmara Fault, and taking a mean recurrence interval of 200 years with a typical coefficient of variation of 0.5, the following conditional probabilities for various exposure times have calculated.

Probability for next 10 yrs: 9.8%
Probability for next 20 yrs: 19%
Probability for next 30 yrs: 27%
Probability for next 40 yrs: 35%
Probability for next 50 yrs: 42%

A comparison for the Poisson and Renewal (Time Dependent) stochastic models for the occurrence probabilities of a large (characteristic) earthquake associated with the fault segments to the south of Istanbul for a 50-year exposure period reveals:

Segment	Mean Rec.Time	Lapse Time	Poisson	Renewal
7-8	250 years	235 years	0.18	0.32
9-10	200-250 years	445 years	0.22	0.50

Where, for the renewal model the frequency density function is modeled as log-normal with a coefficient of variation is taken as 0.5.

These exceptionally high exceedance probabilities, that favorably compares with those reported in Parsons (2000), indicates that it will be prudent to use deterministic approach for the assessment of loses that would result from an impending earthquake in Turkey.
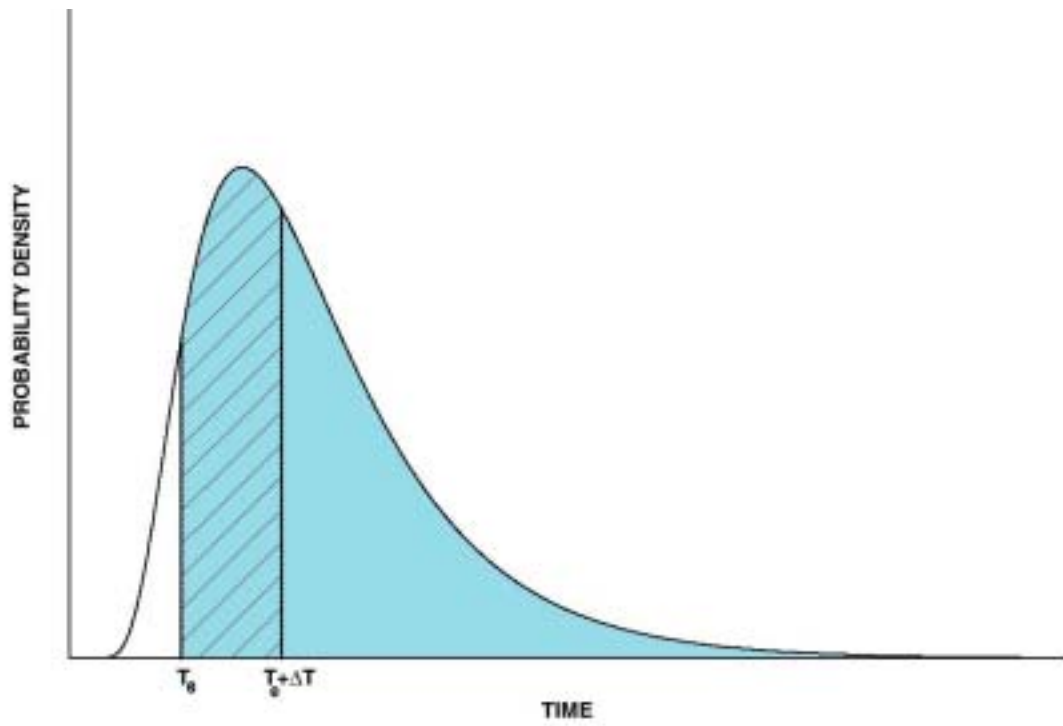
Figure 2.6.1. Calculation of conditional probability from a probability density function.

2.7. DETERMINISTIC EARTHQUAKE HAZARD

Deterministic seismic hazard assessment is conducted to determine the spatial distribution of the earthquake ground motion that would result from a given (scenario) earthquake. The assessment methodology involves: the determination of the scenario earthquake, identification of proper attenuation relationships and appropriate site-response quantification. For this study the deterministic hazard will be evaluated using both intensity based and ground motion (PGA and SA) based attenuation relationships. For both cases median (50-percentile) value obtained from the attenuation relationships were adopted.

2.7.1. Credible Worst Case Scenario (Scenario Earthquake)

The geological and seismological information forms the basis to predict the appropriate scenario earthquake, which is usually given broad terms, involving rupture length, location and the magnitude. In general terms, the earthquake(s) may be associated with local, nearby and distant sources. For "worst case" scenarios the maximum event size is adopted. Scenario earthquake can and has also been defined as the largest earthquake(s) expected in a reasonable period time (generally 500 years). Although, the use of multiple scenario earthquakes can provide for the range of risk mitigation efforts to be planned, it can also decrease the public credibility of the risk assessment. For intrinsically probabilistic applications, the selection of scenario earthquake is based on the deaggregation of the hazard to show which events contribute most to the loss. As such, it will be an event with a high likelihood of occurrence in the source region, relative to other events that can cause the same loss. For Istanbul almost all these procedures converge to a large earthquake associated with the unruptured sections of the Main Marmara Fault passing from south of the city in the Marmara Sea. On these bases and other technical considerations an Mw=7.5 (similar to 1999 Kocaeli earthquake in magnitude and in total rupture length) is selected as the "Credible Worst Case" Scenario event, which is assumed to take place on segments 5,6,7 and 8 as shown in Figure 2.7.1. The segmentation of the northern branch of the North Anatolian Fault in the Marmara Sea can be seen in Figure 2.2.13.

2.7.2. Intensity Based Deterministic Earthquake Hazard

The segmentation of the northern branch of the North Anatolian Fault in the Marmara Sea can be seen in Figure 2.2.13. For the earthquake scenario an Mw=7.5 event is assumed to take place on segments 5,6,7 and 8 as shown in Figure 2.7.1. The intensity attenuation used for this study is based on the regression analysis of the intensity data obtained from Turkish earthquakes (Erdik et. al, 1985) and is favorably compared with the isoseismal map of 1999 Kocaeli earthquake for a magnitude of 7.5 (Figure 2.7.2). Also shown on the same figure are synthetic isoseismal maps that would result from magnitudes of 7.0 and 6.5.

The deterministic modeling of the earthquake hazard in Istanbul in terms of the distribution of site-independent intensities is calculated, based on the intensity attenuation by Erdik et al. (1985), as shown in Figure 2.7.3.

2.7.3. Peak Ground Acceleration and Spectral Acceleration Based Deterministic Earthquake Hazard

For this part of the deterministic hazard assessment study, the selected ground motion parameters of analysis are the Peak Ground Acceleration (PGA) and the Spectral Accelerations (SA) at periods of 0.2 sec and 1 sec. The average of three attenuation

relationships was used for the calculation of the PGA. These were Boore et al. (1997), Campbell (1997) and Sadigh et al. (1997) attenuation relationships. Results of the study are illustrated in Figure 2.7.4, through Figure 2.7.7 for the NEHRP site classes of B, C, D and E-F respectively. The results for site class B can be treated as those to be observed on the so-called engineering bedrock, where shear wave propagation velocity is greater than 760m/s.

The spectral accelerations for T=0.2 sec. and T=1 sec. calculated for NEHRP site class B/C boundary (Vs=760 m/s.) and as the average of Boore et al. (1997) and Sadigh et al. (1997) attenuation relationships are presented in Figure 2.7.8 and Figure 2.7.9. These results will be used as the base values for the application of site-dependent amplification (or de-amplification) factors.

Figure 2.7.1. Mw=7.5 scenario earthquake for Istanbul and vicinity.
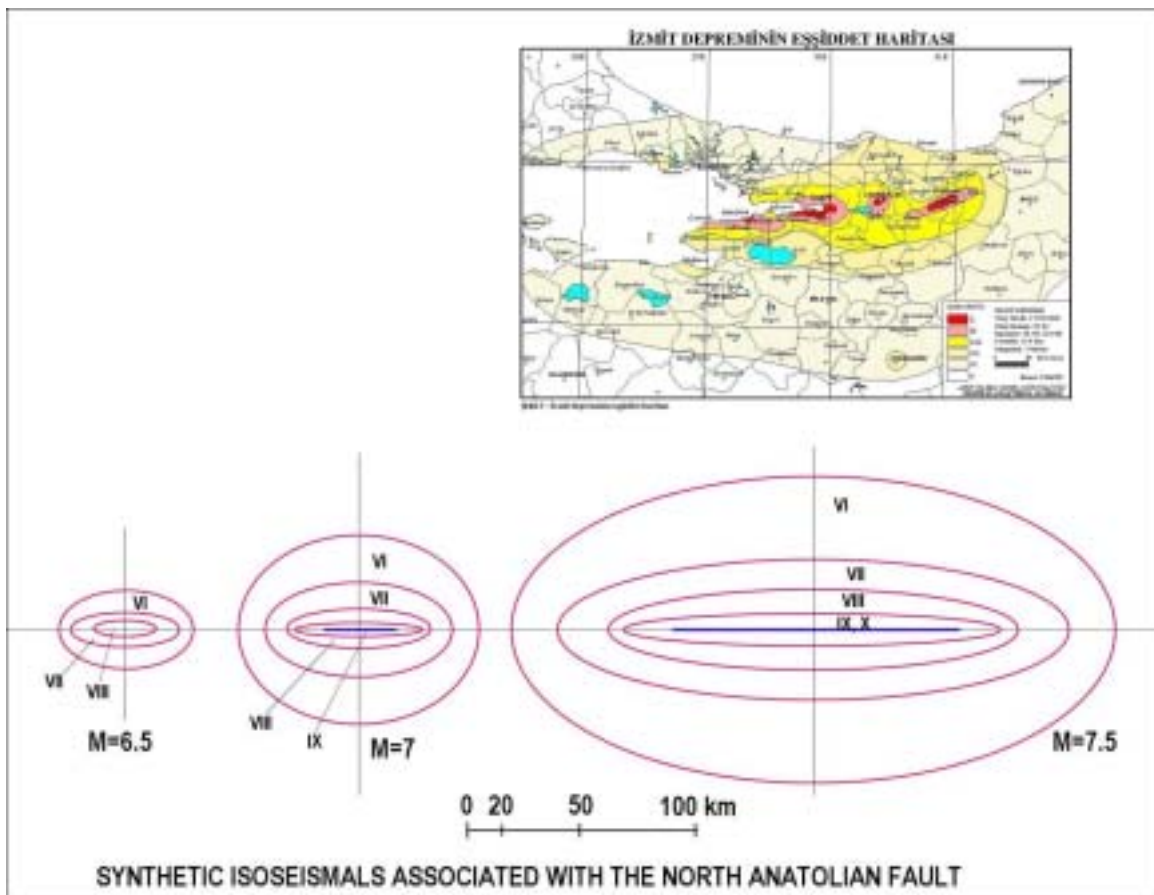
Figure 2.7.2. Comparison of the intensity attenuation relationship with the Isoseismal Map of
Kocaeli Earthquake (Isoseismal Map. After Bulent Ozmen of Gen.Dir.of Disaster Affairs)
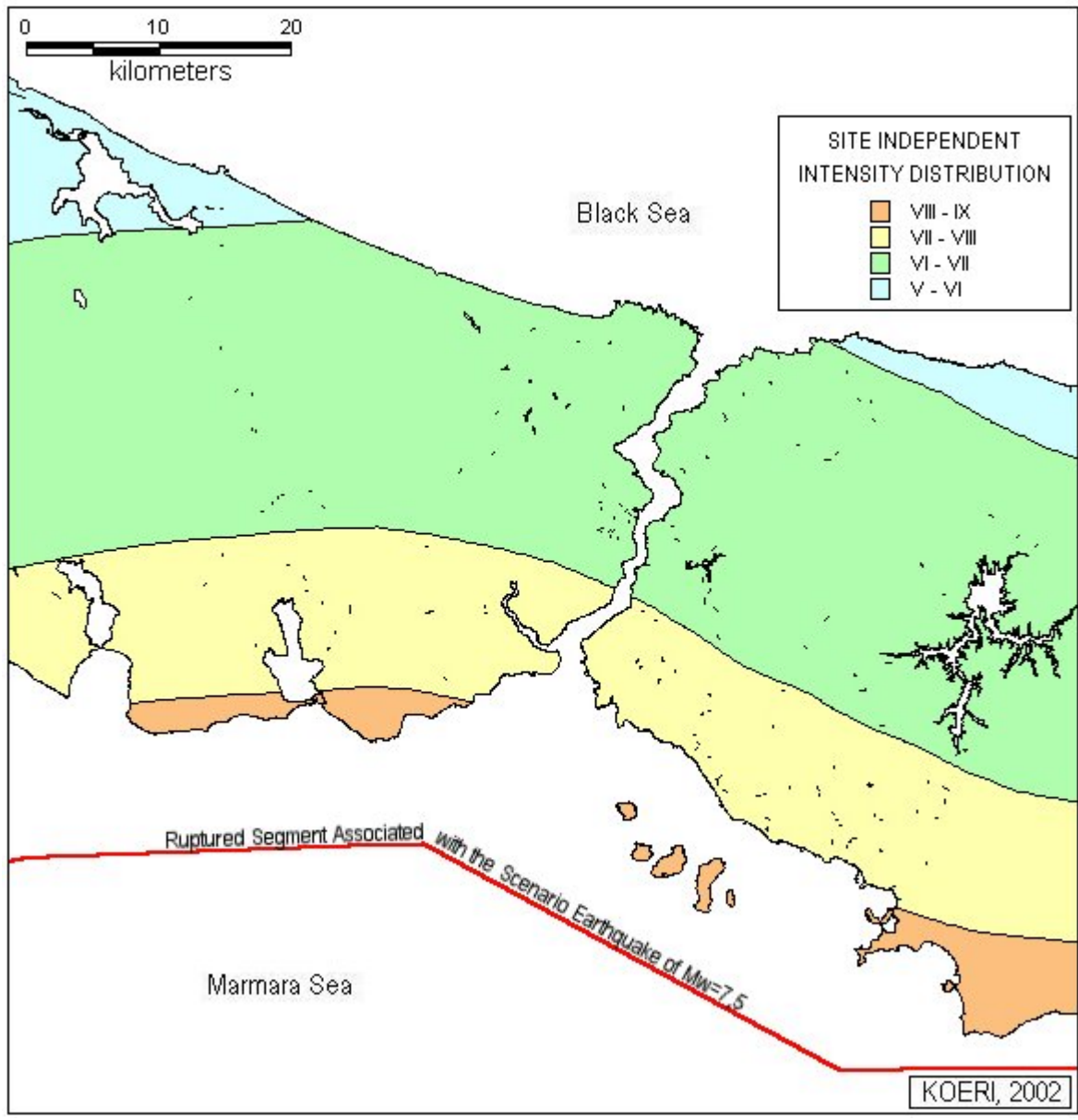
Figure 2.7.3. Site-independent intensities from the Scenanario earthquake
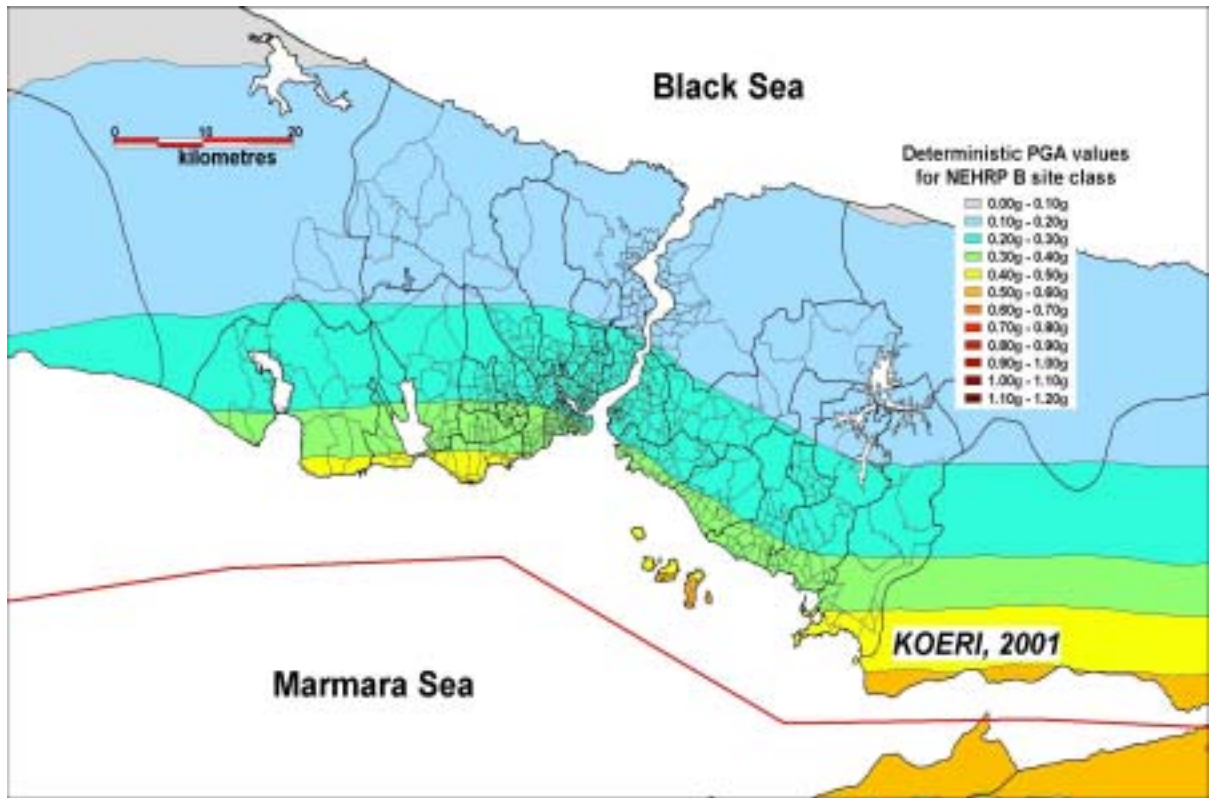
Figure 2.7.4. Deterministic PGA values for NEHRP B site class
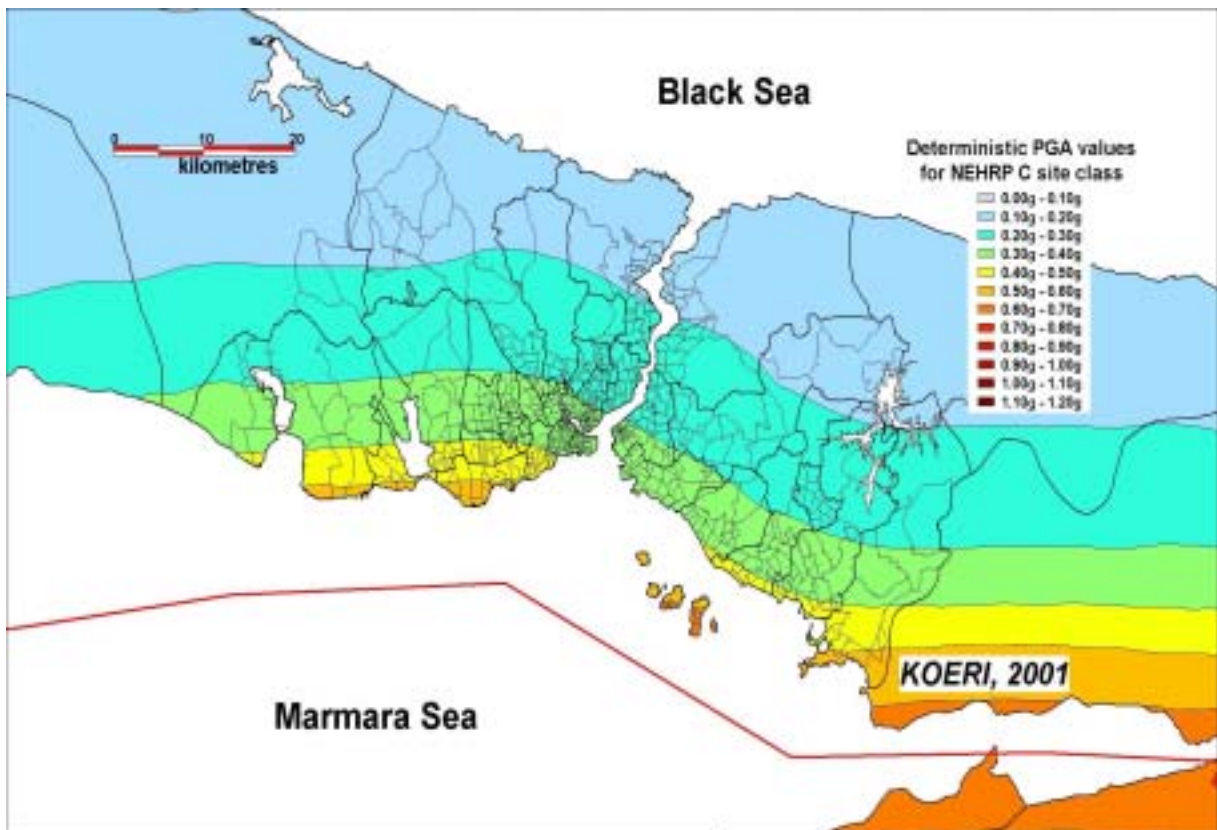
Figure 2.7.5. Deterministic PGA values for NEHRP C site class
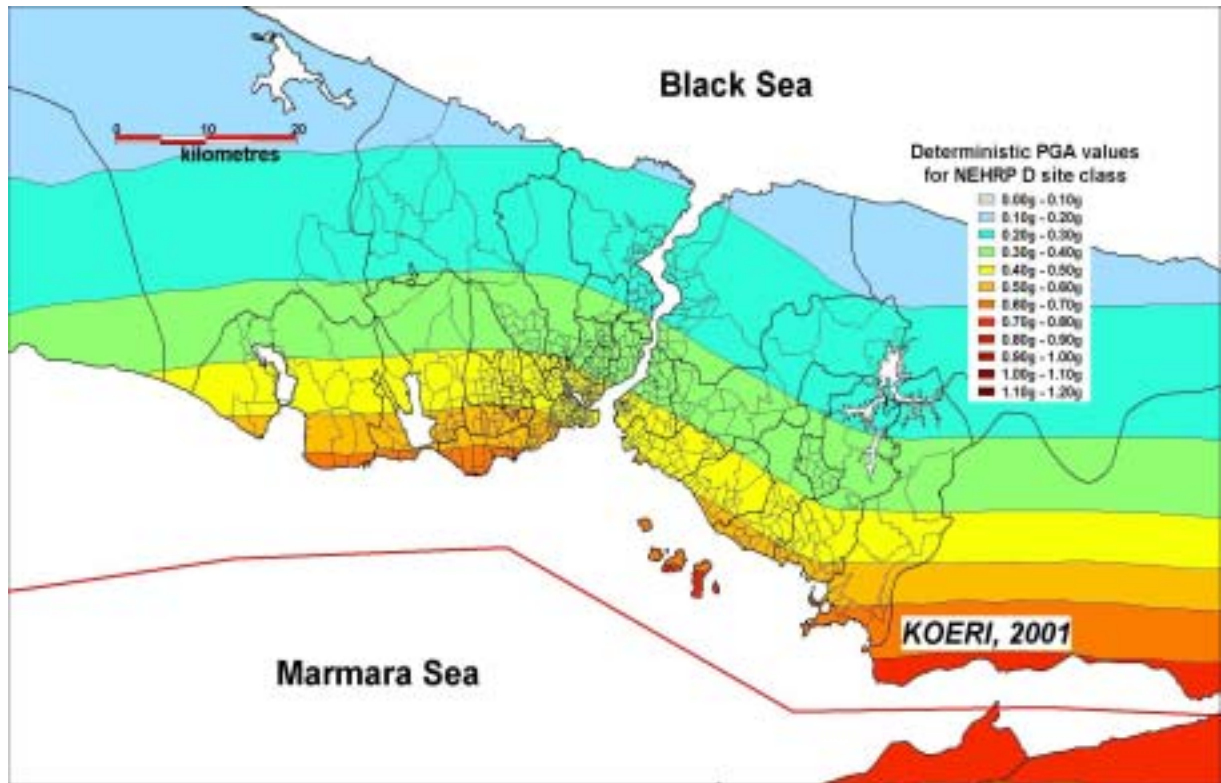
Figure 2.7.6. Deterministic PGA values for NEHRP D site class
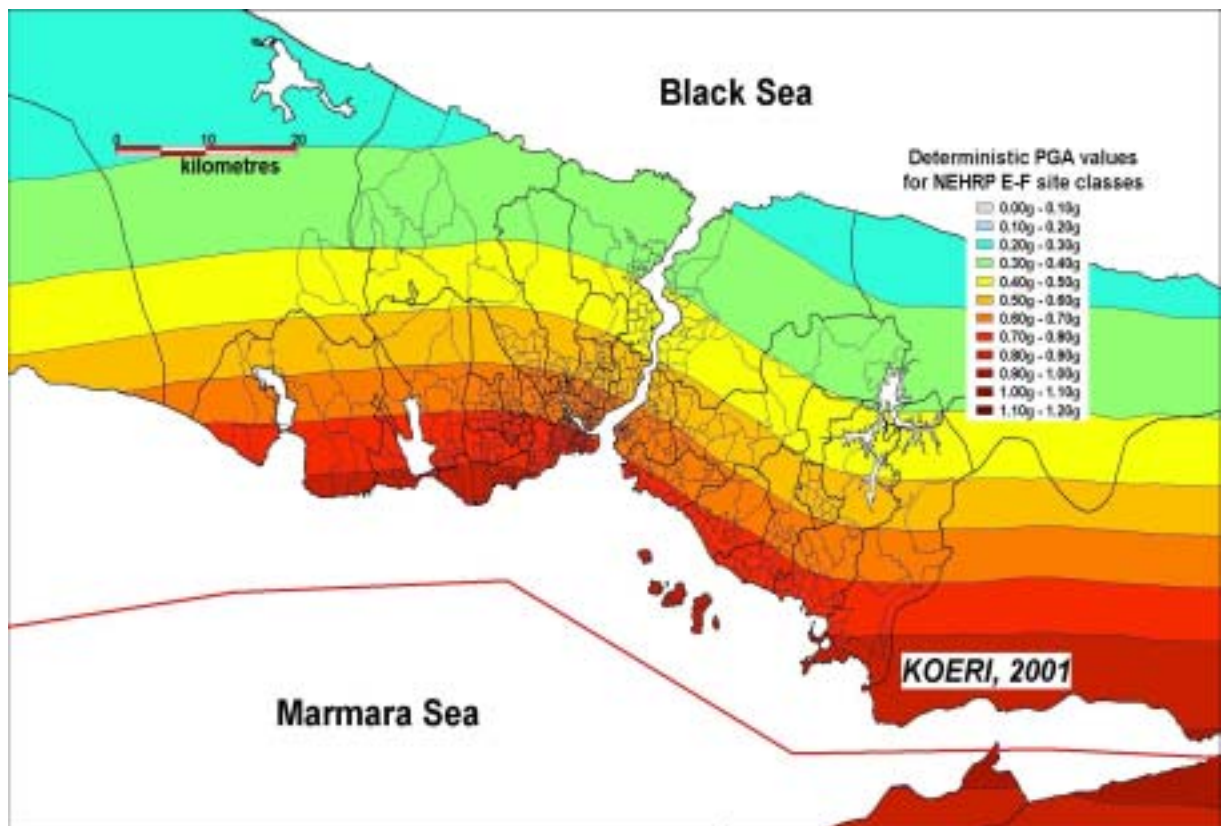
Figure 2.7.7. Deterministic PGA values for NEHRP E-F site class
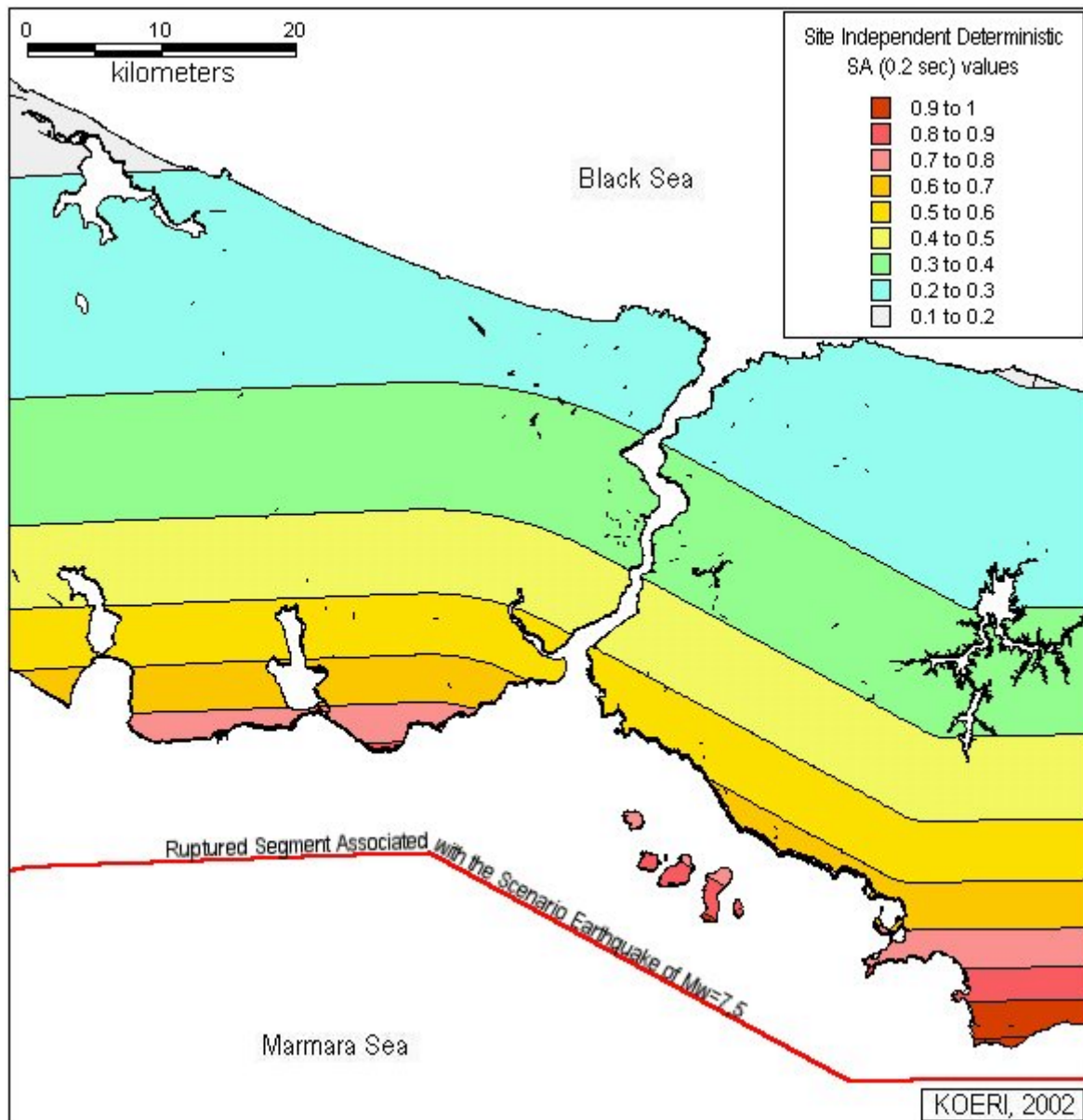
Figure 2.7.8. Deterministic spectral acceleration values (T=0.2 sec.).for NEHRP site class B/C boundary
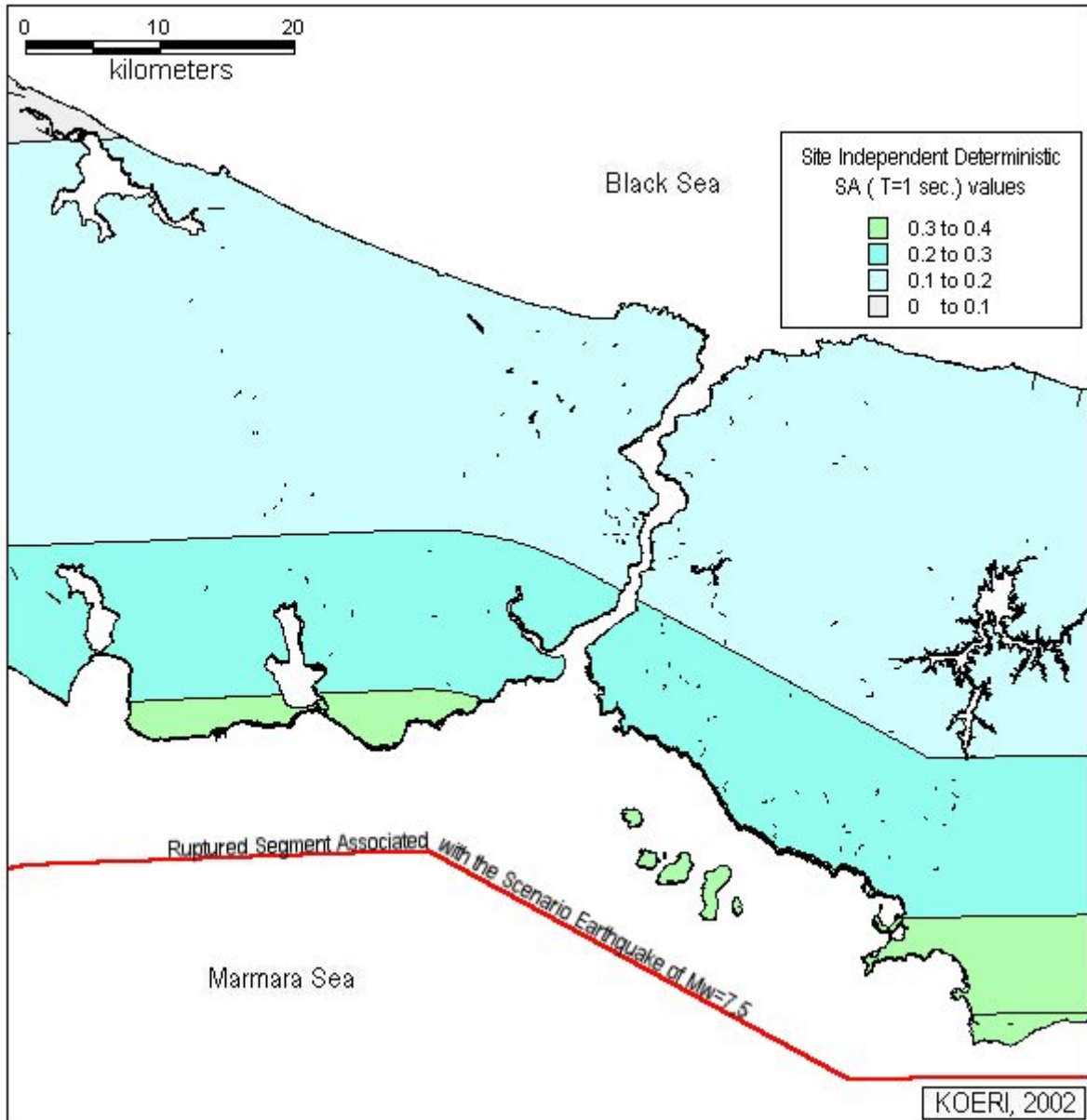
Figure 2.7.9. Deterministic Spectral accelelation values (T=1 sec.).for NEHRP site class B/C boundary

2.8. SITE-SPECIFIC SEISMIC HAZARD

For the quantification of the site effects in the urban earthquake hazard assessment or in earthquake microzonation maps there exist analytical and empirical approaches. Analytical procedures range from simple one-dimensional calculations to three- dimensional, linear/non-linear, time/frequency domain and finite difference/element computations. In general, one-dimensional non-linear analytical procedures are utilized with idealized soil columns. In several blind tests carried out for the examination of these numerical approaches, it has been found that the reliability of any numerical model depend substantially on the measurements of the non-linear characteristics of soils, which inherently exhibit large uncertainties and, furthermore, are expensive to obtain. These facts will tend to prohibit the application of purely analytical-numerical procedures in future developments of earthquake loss scenarios.

In hazard assessments based on empirical intensity attenuations, the modification of the ground motion has been traditionally expressed by some ad-hoc judgmental rules or, preferably, in terms of intensity changes empirically correlated with the ground conditions. Most of the earlier earthquake loss scenario developments in the States have utilized such empirical correlations. In another approach, generally used in Japan, the PGA distributions on competent ground have been computed on the basis of attenuation relationships and then modified on the basis of analytical techniques applied to representative soil profiles. The modified PGA values have then converted to intensity values.

The use of the "Average Horizontal Spectral Amplification" factors sanctioned in NEHRP recommendations provides practical means for incorporation of the average spectral ratio between the horizontal ground motions at a site with respect to a nearby rock site.

Although several investigations have been made corrections to earthquake ground motion parameters for the effects of topography, in routine applications, is very much a matter of judgment at the present time. Although, practical rules exist in some earthquake codes, they have not yet found their way in the development of earthquake loss scenarios

2.8.1. Site Dependent Intensities

The modification of ground motion in terms of intensity has been implemented according to local geological and geotechnical ground conditions of the sites. Table 2.8.1, Table 2.8.2 and Table 2.8.3 provide the variation of intensities for specified geologic site conditions established in several microzonation studies.

Table 2.8.1. Correlation between soil types and intensity increase after Medvedev (1962)

Geological Unit	Intensity Increments
Granites	0
Limestones, sandstone, shales	0.2-1.3
Gypsum, marl	0.6-1.4
Coarse material	1-1.6
Sands	1.2-1.8
Clays	1.2-2.1
Fill	2.3-3.0
Moist Ground (gravel, sand, clay)	1.7-2.8
Moist fill and soil ground (marsh)	3.3-3.9

Table 2.8.2. Correlation of type of rocks and sediments with intensity increments for California (Evernden & Thomson, 1985)

Geological Unit	Intensity Increments
Granitic and metamorphic rocks	0
Paleozoic rocks	0.4
Early Mesozoic rocks	0.8
Cretaceous to Eocene rocks	1.2
Undivided Tertiary rocks	1.3
Oligocene to middle Pliocene rocks	1.5
Pliocene-Pleistocene rocks	2.0
Tertiary volcanic rocks	0.3
Quaternary volcanic rocks	0.3
Alluvium (water table) < 10m	3.0
10-30m	2.0
> 30m	1.0

Table 2.8.3. Correlation between soil type and intensity increment for Japan, JMA intensity scale (Kagami, 1998)

Geological Unit	Intensity Increments
Talus and Andesite	0
Gravel	0.2
River Deposits	0.4
Volcanic Ash	0.5
Sandy Silts	0.7
Clay Silts	0.8
Silt	1.0
Peat	0.9

Table 2.8.4. Intensity increments for each geological unit in Istanbul

Geological Unit	Intensity increments (M.M. scale)
Cavusbasi formation	-0.4
Trakya, Baltalimani, Kurtkoy, Gozdag, Dolayoba, Tuzla, Kartal, Aydos	0.0
Sariyer, Kutluca, Hereke, Sogucak, Hamamdere	0.4
Gurpinar, Karaburun	0.9
Bakirkoy, Gungoren, Cukurcesme, Kusdili, Alluvium	1.1

As explained in Section 2.7.2, the deterministic modeling of the earthquake hazard in Istanbul in terms of the distribution of site-independent intensities is calculated, based on the intensity attenuation by Erdik et al. (1985). Considering that this intensity attenuation has been

assessed for average soil in the region and assuming the average soil denotes NEHRP (1997) B site class for Istanbul region, the intensity map is modified to reflect the influence of geological conditions using the modification rules corrected for soils in Istanbul according to Evernden & Thomson (1985) method. These increments are presented in Table 2.8.4. Site dependent intensities for the Mw=7.5 scenario earthquake are presented in Figure 2.8.1.

2.8.2. Site Dependent Spectral Accelerations

Spectral accelerations (SA) for T=0.2 sec and T=1.0 sec obtained in Section 2.7.3 have been modified according to the site coefficients presented in Table 2.8.4 and 2.8.5 (1997 NEHRP Provisions).

Table 2.8.5. F_a, the short period site-correction defined in the 1994 and 1997 NEHRP Provisions (BSSC, 1995,1998)

Site Class	Ss≤0.25	Ss=0.50	Ss=0.75	Ss=1.0	Ss≥1.25
A	0.8	0.8	0.8	0.8	0.8
B	1	1	1	1	1
C	1.2	1.2	1.1	1	1
D	1.6	1.4	1.2	1.1	1
E	2.5	1.7	1.2	0.9	*
F	*	*	*	*	*

Site-specific geotechnical investigation and dynamic site response analyses shall be performed; shaded area is assigned for this study

Table 2.8.6. F_v, the long period site-correction defined in the 1994 and 1997 NEHRP Provisions (BSSC, 1995,1998)

Site Class	Ss≤0.1	Ss=0.20	Ss=0.3	Ss=0.4	Ss≥0.5
A	0.8	0.8	0.8	0.8	0.8
B	1	1	1	1	1
C	1.7	1.6	1.5	1.4	1.3
D	2.4	2.0	1.8	1.6	1.5
E	3.5	3.2	2.8	2.4	*
F	*	*	*	*	*

The site dependent spectral accelerations for T=0.2 sec and T=1.0 sec are given in Figure 2.8.2 and Figure 2.8.3 respectively.

2.8.3. The inferred ground motion parameters, PGA and PGV

Site dependent peak ground accelerations (PGA) and peak ground velocities (PGV) are calculated using the site dependent spectral accelerations for T=0.2 sec and T=1.0 obtained in Section 2.8.2.

According to the standard response spectrum provided in 1997 NEHRP Provisions the site-specific PGA is defined as 40% of the S_{ms}. Therefore the site dependent PGA values have been calculated by taking 40% of SA at T=0.2. The resulting PGA map is presentedFigure 2.8.4. The process yields comparative results with those obtained with PGA attenuation relationship of Boore et al. (1997), given in Appendix 2. It should be noted that the SA(T=0.2

sec) related PGA definition ma be a more robust definition of PGA as a "yardstick" of ground motion since it is not affected by the sampling interval and data glitches.

Based on HAZUS99 recommendations PGV has been calculated from SA at T=1.0 with the following formula.

$$PGV = \left(\frac{386.4}{2\pi} \cdot S_{A1} \right) / 1.65 \, (2.7) \qquad (2.7)$$

where   PGV is the peak ground velocity in inches per second and
        S_{A1} is the spectral acceleration in units of g, at T=1.0sec.

The resulting PGV have been converted to cm/sec and presented in Figure 2.8.5. The obtained PGV distribution can be compared with those computed from the PGV attenuation relationship given in Joyner and Boore (1988). The PGV attenuation relationship proposed in this paper is as follows:

$$\log y = 2.09 + 0.49(M - 6) - \log r - 0.0026r + 0.17 \qquad (2.8)$$

yielding 20, 30, 55 cm/sec for rock sites and 25, 40, 80 cm/sec for soil sites, for 30, 20 and 10 km respectively. We believe that the SA(1.0 sec) related definition of PGV the variation to soil conditions much better than the PGV attenuation relationships. In very general terms, the contours in the Asian side of Istanbul can be compared with rock site results, while the contours in the European side can be compared with the soil results.
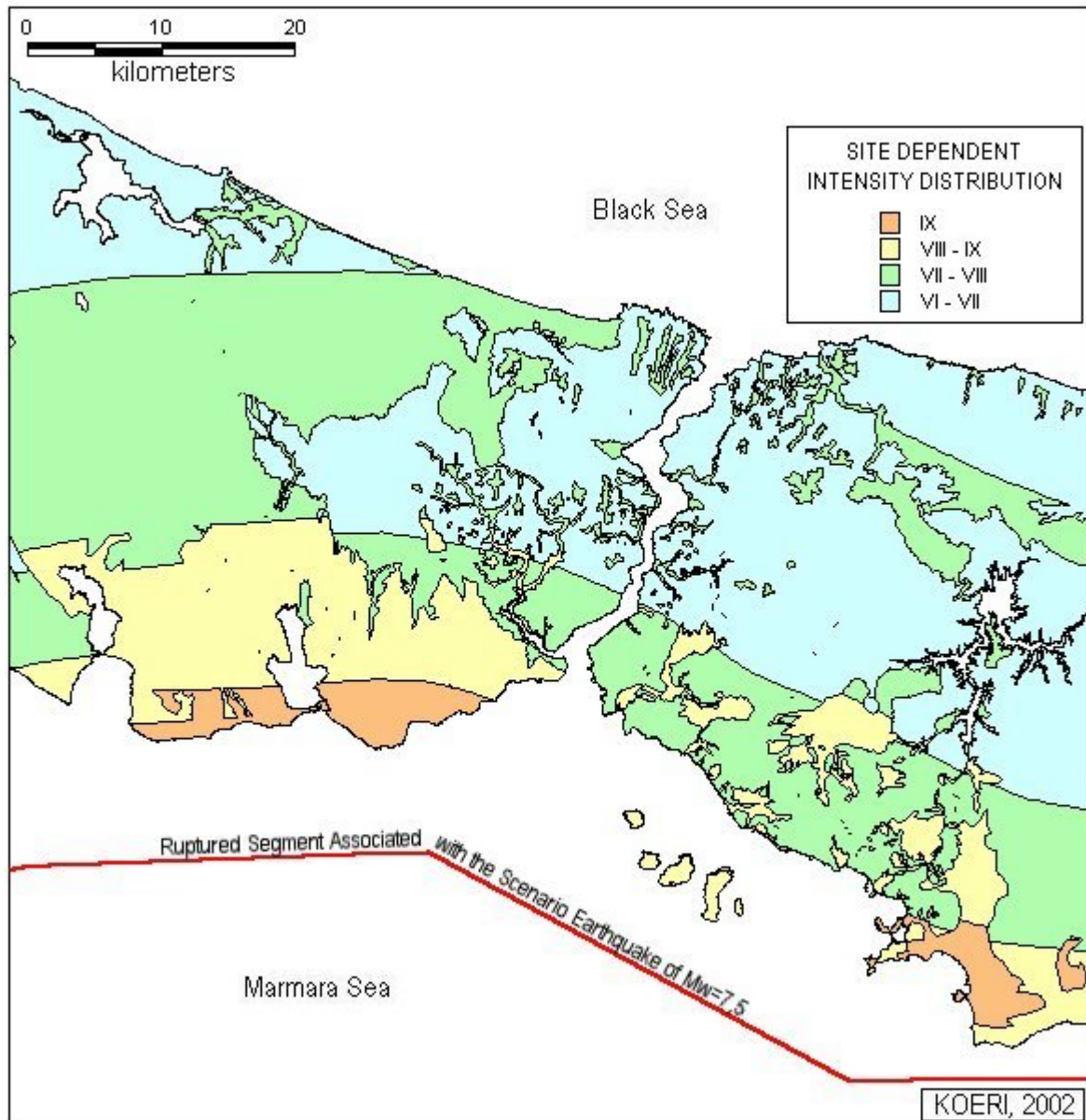
Figure 2.8.1. Site dependent deterministic intensity distribution.
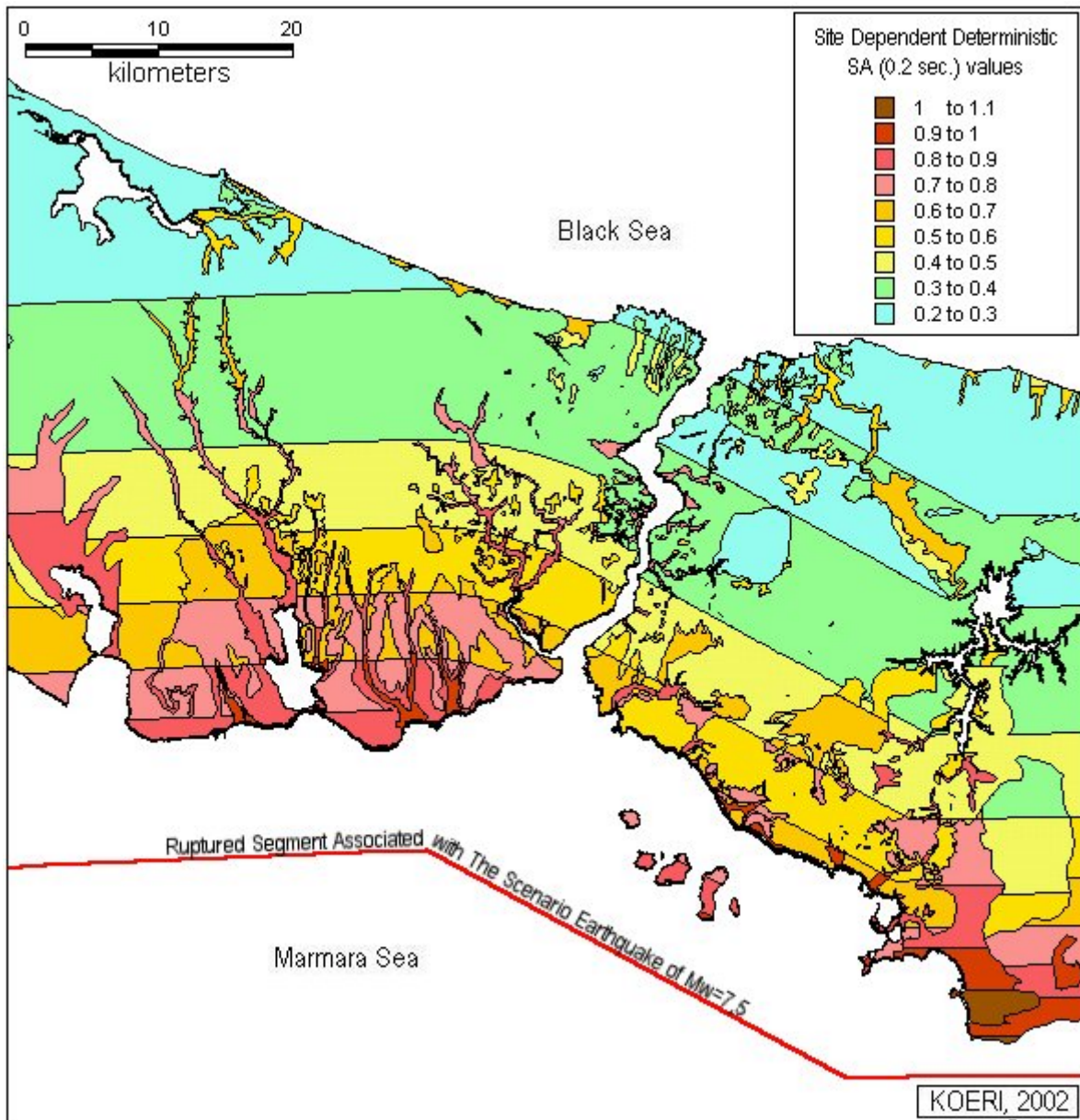
Figure 2.8.2. Site-dependent deterministic SA(T=0.2 sec) values in units of g.
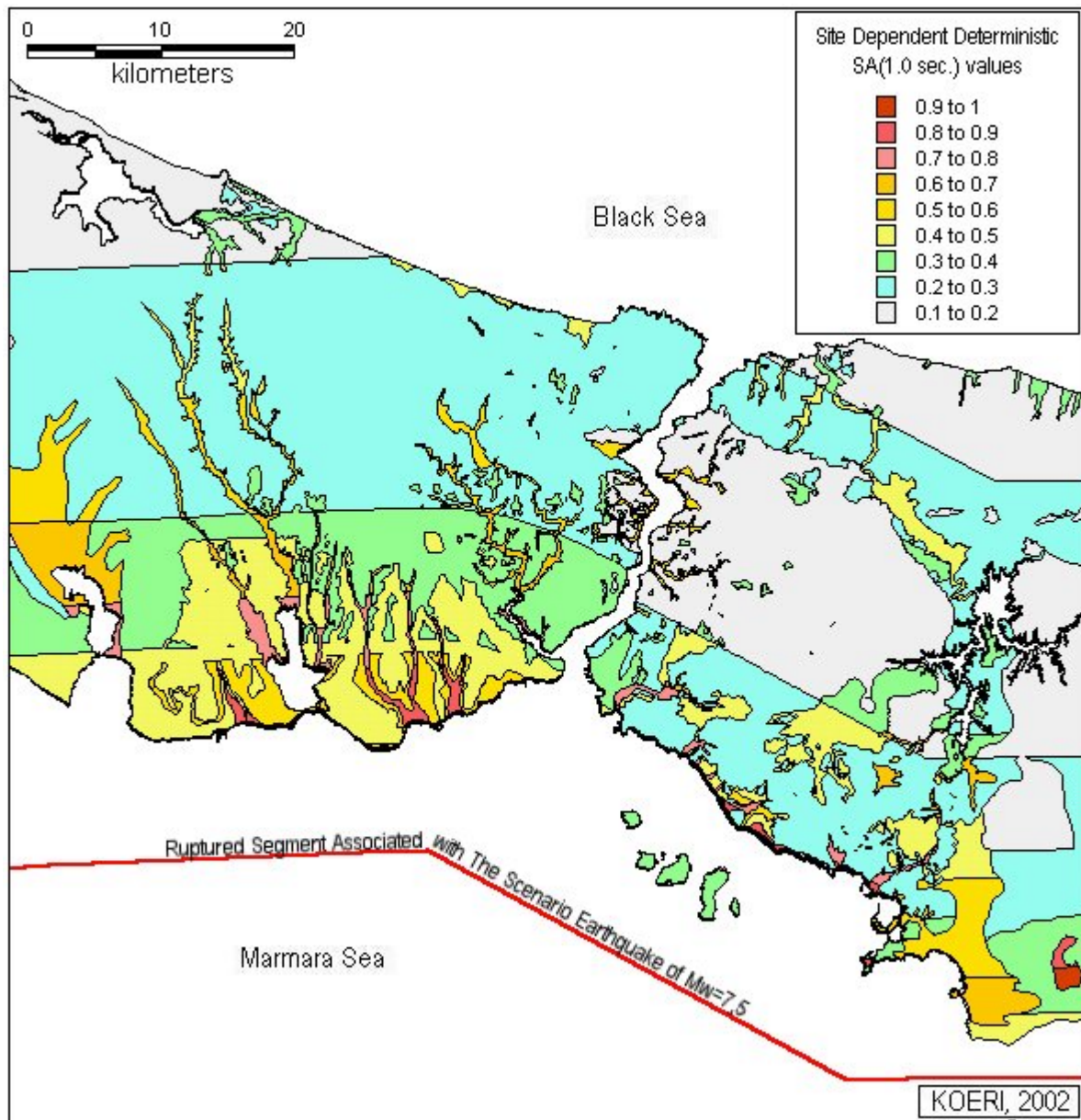
Figure 2.8.3. Site-dependent deterministic SA(T=1.0 sec) values in units of g.
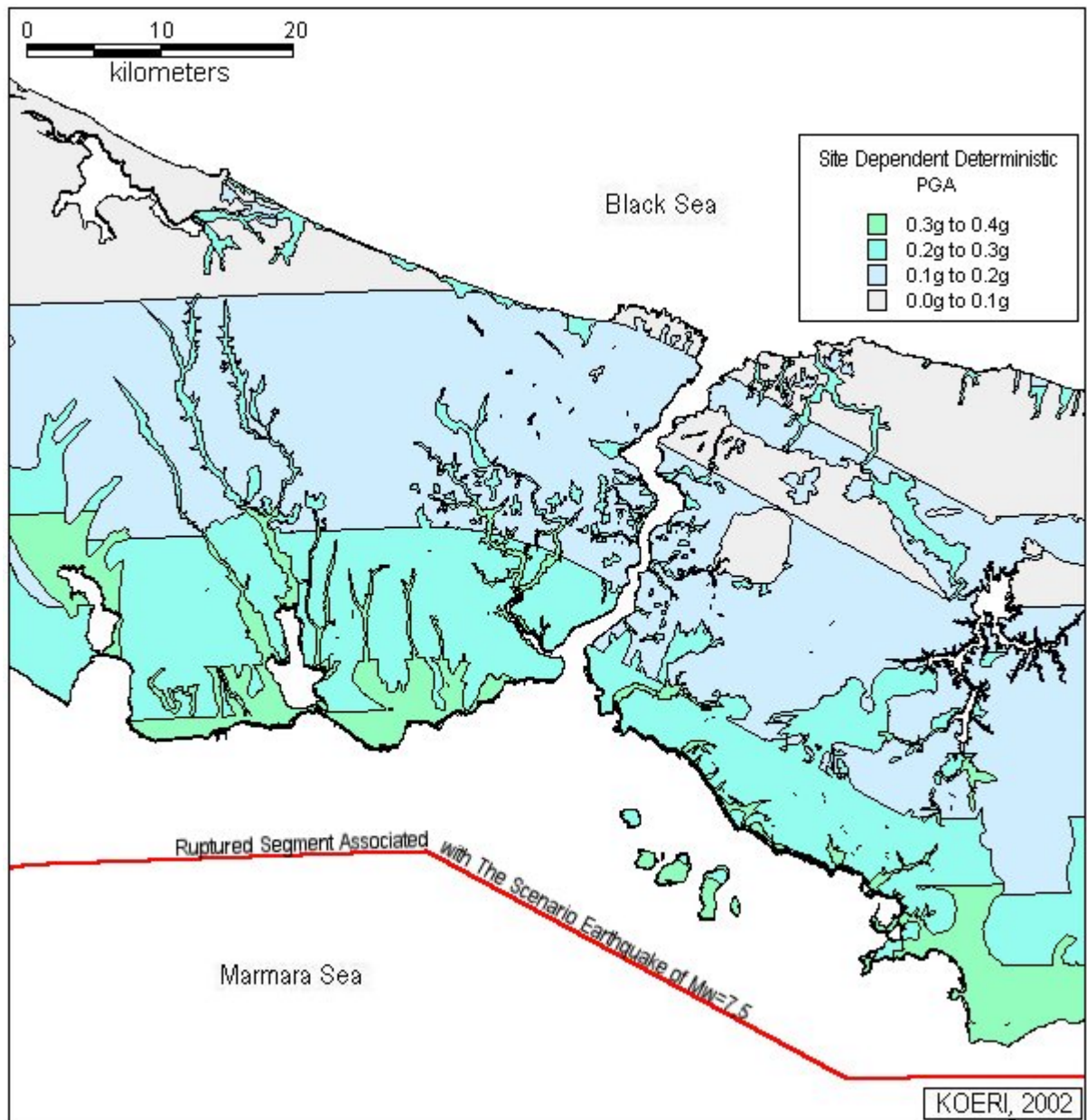
Figure 2.8.4. Site-dependent deterministic PGA values in units of g.
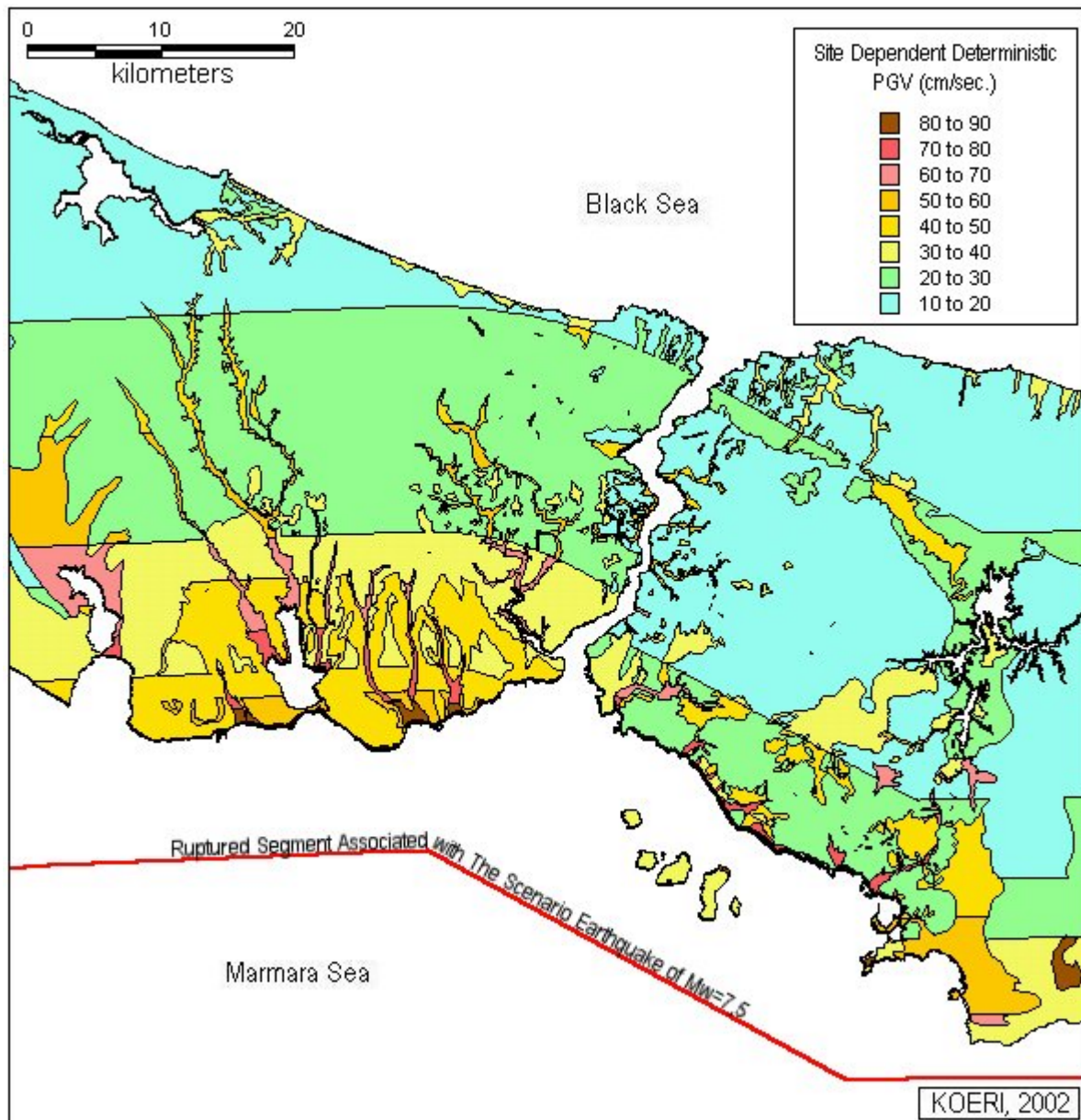
Figure 2.8.5. Site-dependent deterministic PGV values in cm/sec.

REFERENCES

Ambraseys N.N. and J.A. Jackson (2000), Seismicity of the Sea of Marmara (Turkey) since 1500, *Geophys. J. Int.*, 141 F1-F6

Ambraseys, N. N. and C. F. Finkel, (1987a) "The Saros-Marmara earthquake of 9 August 1912", *Earthquake Engineering and Structural Dynamics*, 15, pp: 189-211.

Ambraseys, N. N. and C. F. Finkel, (1987b) "Seismicity of Turkey and Neighboring Regions, 1899-1915", *Annales Geophysicale*, B, 701-726.

Ambraseys, N. N. and C. F. Finkel, (1991), "Long-term seismicity of Istanbul and of the Marmara Sea region", *Terra Nova*, 3, pp: 527-539.

Ambraseys, N.N., (1988), "Engineering Seismology", *Earthquake Engineering and Structural Dynamics*, 17, 1-105.

Armijo R., B. Meyer, A. Hubert, and A. Barka (1999), Westwards Propagation of the North Anatolian Fault into the Northern Aegean: Timing and kinematics, *Geology*, Vol. 27-3, pp. 267-270.

Barka A. A. and K. Kadinsky-Cade, (1988), "Strike-Slip Fault Geometry in Turkey and its influence on earthquake activity", *Tectonics*, Vol. 7, No. 3, pp: 663-684.

Barka, A. A. & R. Reilinger, (1997), "Active tectonics of the Eastern Mediterranean region deduced from GPS, neotectonic and seismicity data", *Annale de Geofisica*. XL, 587-610.

Barka, A. A. & R. Reilinger, (1997), "Active tectonics of the Eastern Mediterranean region deduced from GPS, neotectonic and seismicity data", *Annale de Geofisica*. XL, 587-610.

Barka, A. A., (1992), "The NAFZ", *Annales Tectonicae*, Special issue, Supplement to volume VI, pp: 164-195.

Barka, A. A., (1997), "Neotectonics of the Marmara Region in Active Tectonics of Northwest Anatolia", In: Schindler, C., Pfister, M. (Eds.), *The Marmara Poly-Project*. Hochschule-verlag AG an der ETH, Zurich, pp: 55-87.

Boore, D. M., W. B. Joyner, T. E. Fumal (1997), "Equations for Estimating Horizontal Response Spectra and Peak Acceleration from Western North American Earthquakes: A Summary of Recent Work", Seismological Research Letters, Vol. 68, No. 1, pp. 128-153.

Boore, D., (1983), "Stochastic simulation of high-frequency ground motions based on seismological models of the radiated spectra", *Bull. Seism. Soc. Am.*, 73, 1865-1894.

Borcherdt, R. D., (1994), "Estimates of site-dependent response spectra for design (methodology and justification)", *Earthquake Spectra*, 10, 617-654.

Campbell, K. W. (1997), "Empirical Near-Source Attenuation Relationships for Horizontal and Vertical Components of Peak Ground Acceleration, Peak Ground Velocity, and Pseudo-Absolute Acceleration Response Spectra", *Seismological Research Letters, 68,* January/February.

Cornell C.A., (1968), "Engineering seismic risk analysis", *Bull. Seis. Soc. Amer.*, 58, 1583-1906.

Crampin, S. and R. Evans, (1986), "Neotectonics of the Marmara Sea region of Turkey", *J. Geol. Soc.*, London, 143, pp: 343-346.

Erdik, M., Doyuran, V., Akkas, P. and Gulkan, P., (1985), Assessment of the Earthquake Hazard in Turkey and Neighboring Regions, *Tectonophysics* 117, 295-344.

Erdik,M., Y. Biro, T. Onur, K. Sesetyan and G. Birgoren (1999), "Assessment of earthquake hazard in Turkey and neighboring regions", *Annali Di Geofisica*, Vol. 42 N.6, pp. 1125-1138.

Ergin, K., U. Güçlü and Z. Uz (1967), "A Catalogue of Earthquakes for Turkey and Surrounding Area (11 A.D. to 1964 A.D.)", Istanbul Technical University, Pub. No. 24.

Ergun, M. and E. Ozel, (1995), "Structural relationship between the Sea of Marmara Basin and the North Anatolian Fault Zone", *Terra Nova*, 7, pp: 278-288.

Evernden, J.F. and Thomson, J.M., (1985), Predicting Seismic Intensities, *U.S. Geological Survey Profes. Paper* 1360, pp.151-202.

Eyidogan, H., U. Guclu, Z. Utku, and E. Degirmenci, "Turkiye buyuk depremleri makro-sismik rehberi", ITU, Faculty of Mining, publication of Geophysics Department, 198p, 1991.

Gutenberg, B. & C.F. Richter, (1956), "Earthquake magnitude, intensity, energy and acceleration", *Bull. Seismol. Soc. Am.*, 46, 105-145.

Hartzell, S.H., (1978), "Earthquake aftershocks as Green's functions", *Geophysical Research Letters*, 53, 1425-1436.

Hubert-Ferrari A., A. Barka, E. Jacques, S.N. Nalbant, B. Meyer, R. Armijo, P. Tapponier, and G.C.P. King (2000), Seismic Hazard in the Marmara Sea Region Following the 17 August 1999 İzmit Earthquake, *Nature*, Vol 404.

Joyner, W. B. and D. M. Boore (1988), "Measurement, Characterization, and Prediction of Strong Ground Motion", *Proceedings of Earthquake Engineering and Soil Dynamics II*, GT DIV/ASCE, Park City Utah, June 27-30, 1988, pp.43-102.

Kagami,H., Okada, S. and Ohta, Y., (1988), "Versatile Application of Dense and Precision Seismic Intensity Data by an Advanced Questionnaire Survey", *Proc. Ninth World Conf. on Earthquake Engineering*, Vol.8, pp.937-942.

Ketin, I and F. Roesli (1953), "Makroseismische Untersuchgen über das nordwest-anatolische Beben vom 18 marz 1953", *Ecologas Geol. Helv.*, 46, 187-208.

Kudo, K., T. Kanno, H. Okada, O. Ozel, M. Erdik, M. Takahashi, T. Sasatani, S. Higashi, & K. Yoshida, (2000), "Site Specific Issues on Strong Ground Motion during the Kocaeli, Turkey Earthquake of August 17, 1999, as Inferred from Array Observations of Microtremors and Aftershocks" submitted to *BSSA Special Issue* (August 10, 2000).

Le Pichon, X, A.M.C. Sengör, E. Demirbag, C. Rangin, C. Imren, R. Armijo, N. Görür, N. Çagatay, B. Mercier de Lepinay, B. Meyer, R. Saatçilar and B. Tok ,(2001), "The Active Main Marmara Fault", Earth and Planetary Science Letters, Vol. 192 (4) pp. 595-616.

Leyendecker, E.V., R.J. Hunt, A.D. Frankel, & K.S. Rukstales, (2000), "Development of Maximum Considered Earthquake Ground Motion Maps", *Spectra*, Earthquake Engineering Research Institute, Oakland.

Medvedev, J., (1962), "Engineering Seismology", Academia Nauk Press, Moscow, 260pp.

NEHRP (1997), "Recommended Provisions For Seismic Regulations For New Buildings and Other Structures, FEMA-303", Prepared by the Building Seismic Safety Council for the Federal Emergency Management Agency, Washington, DC.

Ozalaybey, S. H. Karabulut, M. Ergin, M. Aktar, M. Bouchon (2001), "The 1999 Izmit earthquake sequence in NW-Turkey seismological aspects", *Symposia on Seismotectonics of te Northwestern Anatolia-Aegean and Recent Turkish Earthquakes,* ITU, Istanbul.

Ozbey C. (2001), "Empirical Peak Horizontal Acceleration Attenuation Relationship for Northwestern Turkey", M.Sc. Thesis, KOERI, Bogazici University.

Ozbey, C, (2002), Internal Report, KOERI, Boğazici University.

Ozel, O., E. Cranswick, M. Meremonte, M. Erdik and E. Safak (2002) "Site Effects in Avcilar, West of Istanbul, Turkey from Strong and Weak Motion Data" *BSSA*, 92, pp. 499-508.

Oztin, F., "9 Ağustos 1912 Şarköy-Mürefte depremi", *Bull. Earthquake Res. (Deprem Araştırma Bulteni)*, 56, pp: 91-127, 1987.

Papazachos, B.C, (1996), "Seismicity of the Aegean and surrounding area", *Tectonophysics*, 178-287-308.

Parsons, T, R. S. Stein, R. W. Simpson, P. A. Reasenberg, (1999) "Stress sensitivity of fault seismicity: A comparison between limited-offset oblique and major strike-slip faults**",** *J. Geophys. Res.* 104.

Pfannenstiel, M., (1944), "Diluviale Geologie des Mittelmeergebietes: die diluvialen Entwicklungstadien und die Urgeschichte von Dardanellen, Marmara Meer und Bosphorus", *Geol. Rund.*, 34, pp: 342-334.

Pinar, N., (1943), "Marmara denizi havzasının sismik jeolojisi ve meteorolojisi", *Science Faculty Monographies*, A7, 64 p.

Sadigh, K.,C.Y.Chang,J.A.Egan, F. Makdisi, R.R.Youngs (1997), "Attenuation Relationships for Shallow Crustal Earthquakes Based on California Strong Motion Data", Seismological Research Letters, 68, pp. 180-189.

Saroğlu, F., O. Emre and I. Kuscu (1992), "Active Fault Map of Turkey", Mineral Res. Explor. Inst. Turkey.

Sengor, A. M. C., (1987), "Cross-faults and differential stretching of hanging walls in regions of low angle normal faulting: Examples from Western Turkey", in: *Continental Extensional Tectonics*, edited by: M. P. Coward, J. F. Dewey and P. L. Hancock, Geological Society, London, Special Publication, No: 28, pp: 575-589.

Somerville, P.G., and Yoshimura, J., 1990. "The Influences of Critical Moho Reflections on Strong Ground Motions Recorded in San Francisco and Oakland During the 1989 Loma Prieta Earthquake" in *Geophysics Research Letters*, v. 17, pp. 1203-1206.

Somerville, P.G., N.F. Smith, R.W. Graves, & N.A. Abrahamson, (1997), "Modification of empirical strong ground motion attenuation relations to include the amplitude and duration effects of rupture directivity", *Seismological Research Letters*, 68: 199-222.

Stepp, J. C., (1973), "Analysis of completeness of the earthquake sample in the Puget Sound area". in Harding, S. T., Editor, Contributions to seismic zoning: *U.S. National Oceanic and Atmospheric Administration Technical Report* ERL 267-ESL 30, p. 16-28.

Straub, C., H.-G. Kahle, and C. Schindler, (1997), "GPS and Geologic Estimates of the Tectonic Activity in the Marmara Sea region, NW Anatolia", *Journal of Geophysical Research*, Vol. 102, No. B12, pp: 27,587-27,601, Dec. 10.

Trifonov, V.G. & M.N. Machette, (1993), " The world map of major active faults project", *Annali di Geofisica*, 36, 225-236.

Wald, D.J., Quitoriano, V., Heaton, T.H., Kanamori, H., Scrivner, C.W., Worden, C.B., (1999), TriNet "ShakeMaps": Rapid Generation of Peak Ground Motion and Intensity Maps for Earthquakes in Southern California, *Earthquake Spectra*, Vol.15, No.3, pp.537-555.

Westaway, R., (1990). "Block rotation in western Turkey and elsewhere, Theoretical models", J.G.R., Vol. 95., B12, 19885-19901.

Wilson,R., Eieczorek, G. and Harp, E. (1979), Development of Criteria for Regional Mapping of Seismic Slope Stability, *1979 Annual Meeting of the Geological Society of America*.

Wong H. K., T. Ludmann, A. Uluğ, and N. Gorur, (1995), "The Sea of Marmara: A Plate Boundary Sea in an escape tectonic regime", *Tectonophysics*, 244, pp: 231-250, Elsevier Science.

Youd, L., and Perkins, D.M., (1978), Mapping of Liquefaction Induced Ground Failure Potential, *J. GED, ASCE*, Vol. 104, No.4, pp.433-446.